

GraphBench: Next-generation graph learning benchmarking

Timo Stoll^{*1}, Chendi Qian^{*1}, Ben Finkelshtein^{*2}, Ali Parviz^{*3}, Darius Weber^{*1}, Fabrizio Frasca^{*4}, Hadar Shavit^{*1}, Antoine Siraudin^{*1}, Arman Mielke^{*5,6}, Marie Anastacio^{*1}, Erik Müller^{*1}, Maya Bechler-Speicher⁷, Michael Bronstein^{2,8}, Mikhail Galkin⁹, Holger Hoos¹, Mathias Niepert⁶, Bryan Perozzi⁹, Jan Tönshoff¹⁰, and Christopher Morris^{†1}

¹RWTH Aachen University

²University of Oxford

³Mila – Quebec AI Institute

⁴Technion - Israel Institute of Technology

⁵ETAS Research

⁶University of Stuttgart

⁷Meta

⁸AITHYRA

⁹Google Research

¹⁰Microsoft Research

Machine learning on graphs has recently achieved impressive progress in various domains, including molecular property prediction and chip design. However, benchmarking practices remain fragmented, often relying on narrow, task-specific datasets and inconsistent evaluation protocols, which hampers reproducibility and broader progress. To address this, we introduce GRAPHBENCH, a comprehensive benchmarking suite that spans diverse domains and prediction tasks, including node-level, edge-level, graph-level, and generative settings. GRAPHBENCH provides standardized evaluation protocols—with consistent dataset splits and performance metrics that account for out-of-distribution generalization—as well as a unified hyperparameter tuning framework. Additionally, we benchmark GRAPHBENCH using message-passing neural networks and graph transformer models, providing principled baselines and establishing a reference performance. See www.graphbench.io for further details.

^{*}First author, order decided randomly.

[†]Main contributing senior author.

1. Introduction

Machine learning on graphs using *graph neural networks* (GNNs), specifically *message-passing neural networks* (MPNNs) [Gilmer et al., 2017, Scarselli et al., 2009] and *graph transformers* (GTs) [Müller et al., 2024a], has become a cornerstone of modern machine learning research, spanning applications in drug design [Wong et al., 2023], recommender systems [Ying et al., 2018], chip design [Zheng et al., 2025], and combinatorial optimization [Cappart et al., 2021]. Despite these advances, benchmarking in the field remains highly fragmented. Narrow, task-specific datasets and inconsistent evaluation protocols limit reproducibility and hinder meaningful comparison across tasks and domains [Bechler-Speicher et al., 2025]. As Bechler-Speicher et al. [2025] argue, current benchmarks tend to emphasize specific domains—such as 2D molecular graphs—while overlooking more impactful, real-world applications like relational databases, chip design, and combinatorial optimization. Many benchmark datasets fail to accurately reflect the complexity of real-world structures, resulting in inadequate abstractions and misaligned use cases. In addition, the field’s heavy reliance on accuracy as a primary metric encourages overfitting, rather than fostering generalizable, robust models. As a result, these limitations have significantly hindered progress in graph learning.

Shortcomings of current most-used graph learning datasets Existing graph benchmarks have driven progress through standardized datasets and evaluations, but suffer from key limitations. TUDATASETS [Morris et al., 2020] introduced many graph-level tasks, yet most are small, molecular, and lack unified metrics, hindering comparability. The *Open Graph Benchmark* (OGB) [Hu et al., 2020a] and its extensions [Hu et al., 2021] provide large-scale datasets; however, they focus heavily on molecules, require substantial computational resources, and lack clear broader relevance. Other efforts, such as Dwivedi et al. [2020] and the *Long-range Graph Benchmark* (LRGB) [Dwivedi et al., 2022a], emphasize narrow prediction regimes, small-scale data, and restricted model sizes, with limited evaluation of out-of-distribution generalization. Benchmarks for graph generation remain underdeveloped [Bechler-Speicher et al., 2025], often relying on 2D molecular datasets with questionable practical value, synthetic data with limited applicability, and tasks that fail to address challenges such as generating large or structurally constrained graphs. Recent work has sought to formalize dataset quality assessment [Coupette et al., 2025] and expand node-level tasks with GRAPHLAND [Bazhenov et al., 2025], but scalability and coverage gaps remain.

Present work We introduce GRAPHBENCH, a next-generation benchmarking suite addressing key shortcomings in graph learning evaluation. GRAPHBENCH spans diverse domains—algorithmic reasoning, chip design, combinatorial optimization, SAT solver prediction, social networks, and weather forecasting—and supports node-, edge-, graph-level, and generative tasks. It provides standardized splits, domain-specific metrics, and hyperparameter-tuning scripts, along with out-of-distribution evaluation for selected datasets to assess generalization. We benchmark modern MPNNs and graph transformers, offering strong baselines and insights into architectural trade-offs. *By unifying heterogeneous tasks under one framework, GRAPHBENCH enables reproducible, robust, and impactful graph learning research, see Figure 1, paving the way for graph foundation models.*

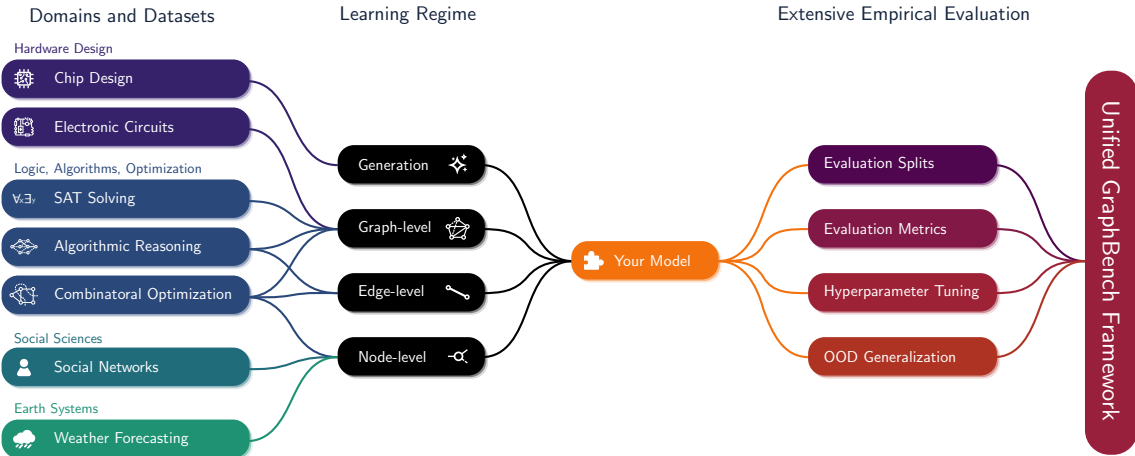


Figure 1: **Overview of the GraphBench framework.** GRAPHBENCH integrates diverse **domain datasets**—ranging from social sciences and hardware design to logic, optimization, and earth systems—into different *learning regimes* (node-, edge-, graph-level prediction and generative tasks). GRAPHBENCH offers *extensive empirical evaluation* via standardized splits, metrics, hyperparameter tuning scripts, and out-of-distribution (OOD) generalization tests, all within a *unified evaluation pipeline*.

2. Overview of GraphBench

The goal of GRAPHBENCH is to support the next generation of graph learning research by addressing key shortcomings of existing benchmarks. Here, we provide an overview of the design and features of GRAPHBENCH. GRAPHBENCH provides a unified framework for evaluating models across diverse graph tasks, domains, and data scales. Unlike previous benchmarks that focus narrowly on specific applications (e.g., molecular graphs or citation networks), with little (industrial or real-world) impact, GRAPHBENCH includes datasets from *social networks*, *chip design*, *combinatorial optimization*, *SAT solving*, and more.

GRAPHBENCH is designed around the following core principles.

1. **Diverse tasks and domains** GRAPHBENCH supports node-, edge-, and graph-level prediction, as well as generative tasks. Datasets span diverse domains, including social networks, chip and analog circuit design, algorithm performance prediction, and weather forecasting. This diversity enables the evaluation of models in both traditional and emerging graph learning applications.
2. **Real-world impact** Many existing benchmark suites focus on small-scale graphs or domains that have limited applicability to current real-world challenges. In contrast, GRAPHBENCH emphasizes datasets and tasks that are more representative of modern real-world use cases, such as large-scale chip design, weather forecasting, and combinatorial optimization. By moving beyond the citation network- and molecular-dominated domains of prior benchmarks, GRAPHBENCH offers scenarios that better align with the needs of industry and emerging research areas.
3. **OOD generalization** Several datasets in GRAPHBENCH are explicitly split by time or problem size to test a model’s ability to generalize beyond the training distribution. For instance, social network benchmarks assess future interaction prediction using only past data, while circuit

Table 1: Summary of currently available GRAPHBENCH datasets.

Category	Name	Node Feat.	Edge Feat.	Directed	Hetero	#Tasks	Split Scheme	Split Ratio	Task Type	Metric
Social networks	BlueSky – quotes	✓	–	✓	–	3	Temporal	(55/15)/15/15	Node regression	MAE / R ² / Spearman corr.
	BlueSky – replies	✓	–	✓	–	3	Temporal	(55/15)/15/15	Node regression	MAE / R ² / Spearman corr.
	BlueSky – reposts	✓	–	✓	–	3	Temporal	(55/15)/15/15	Node regression	MAE / R ² / Spearman corr.
Chip design	AIG	✓	✓	✓	–	1	Fixed	80/10/10	Generation	Ad-hoc Score
Electronic circuits	5 Components	✓	–	–	–	1	Random	70/10/20	Regression	RSE
	7 Components	✓	–	–	–	1	Random	70/10/20	Regression	RSE
	10 Components	✓	–	–	–	1	Random	70/10/20	Regression	RSE
SAT Solving	SMALL	–	–	–	✓\–	5	Fixed	80/10/10	Classification / Regression	Closed Gap / RMSE
	MEDIUM	–	–	–	✓\–	5	Fixed	80/10/10	Classification / Regression	Closed Gap / RMSE
	LARGE	–	–	–	✓\–	5	Fixed	80/10/10	Classification / Regression	Closed Gap / RMSE
Combinatorial optimization	RB – Small	–	–	–	–	6	Fixed	70/15/15	Regression / Unsupervised	MAE / CO
	RB – Large	–	–	–	–	6	Fixed	70/15/15	Regression / Unsupervised	MAE / CO
	ER – Small	–	–	–	–	6	Fixed	70/15/15	Regression / Unsupervised	MAE / CO
	ER – Large	–	–	–	–	6	Fixed	70/15/15	Regression / Unsupervised	MAE / CO
	BA – Small	–	–	–	–	6	Fixed	70/15/15	Regression / Unsupervised	MAE / CO
	BA – Large	–	–	–	–	6	Fixed	70/15/15	Regression / Unsupervised	MAE / CO
Algorithmic reasoning	Topological Sorting	✓	✓	✓	–	3	Fixed	98/1/1	Node regression	MAE
	MST	–	✓	–	–	3	Fixed	98/1/1	Edge classification	Accuracy / F1
	Bridges	–	–	–	–	3	Fixed	98/1/1	Edge classification	Accuracy / F1
	Steiner Trees	✓	✓	–	–	3	Fixed	98/1/1	Edge classification	Accuracy / F1
	Max Clique	–	–	–	–	3	Fixed	98/1/1	Node classification	Accuracy / F1
	Flow	✓	✓	✓	–	3	Fixed	98/1/1	Regression	MAE
Weather forecasting	Max Matching	–	✓	–	–	3	Fixed	98/1/1	Edge classification	Accuracy / F1
	ERA5 64x32	✓	✓	✓\–	–	1	Temporal	86/5/9	Node regression	MSE

benchmarks evaluate generalization across different circuit sizes.

- 4. Meaningful evaluation** GRAPHBENCH provides evaluation splits, meaningful domain-specific evaluation metrics, and state-of-the-art hyperparameter tuning scripts. In addition, we offer out-of-distribution generalization evaluation for selected datasets, focusing on size generalization abilities, paving the way for graph foundation models.
- 5. Task-relevant evaluation metric** GRAPHBENCH provides metrics tailored to each task that capture models’ real-world performance. These measures extend beyond classical metrics such as mean-squared error and accuracy, which may not accurately reflect practical utility in real-world scenarios.

Benchmarks and evaluation To facilitate fair and reproducible comparisons, GRAPHBENCH offers a comprehensive benchmarking protocol for each dataset, including (i) a clearly defined prediction or generation task (e.g., node-, link-, or graph-level classification/regression, or graph generation), (ii) a realistic and domain-appropriate data split strategy (e.g., temporal splits for social networks, cross-size splits for electronic circuits), (iii) standardized input features and labels to ensure consistency across models, and (iv) evaluation scripts implementing task-specific metrics (e.g., RMSE, ROC-AUC, closed gap) along with state-of-the-art hyperparameter tuning scripts. This standardized setup enables researchers to compare methods under realistic conditions while reducing the burden of dataset curation and preprocessing.

Baselines and experimental evaluation To establish strong reference points, we evaluate a range of graph learning architectures, including MPNNs and graph transformers. All are evaluated across multiple random seeds to assess robustness. Our empirical analysis reveals persistent challenges for current methods, including coping with temporal distribution shifts and maintaining efficiency during training on graph-structured data.

Software and accessibility **GRAPHBENCH** is released as an open-source, user-friendly **PYTHON** package designed for ease of adoption and extension.¹ It provides streamlined data loaders and **PYTORCH GEOMETRIC**-based data objects, predefined training, validation, and test splits for each dataset, and ready-to-use state-of-the-art hyperparameter tuning scripts. Its modular design allows practitioners and researchers to rapidly prototype, benchmark, and deploy new graph learning models while adhering to a unified evaluation protocol; see Section 2.1 below for an example of using **GRAPHBENCH**’s interface.

2.1. Example usage of GraphBench

We provide a unified and easy-to-use interface for **GRAPHBENCH** datasets. Inspired by benchmarks such as OGB [Hu et al., 2020a] and LRGB [Dwivedi et al., 2022a], we use wrapper methods to handle dataset loading. Unlike competing benchmarks, however, **GRAPHBENCH** offers a single loading class (`graphbench.Loader`) for all datasets, independent of task type. Each wrapper includes the necessary precomputations and comes with predefined splits, enabling direct use in downstream tasks. Nonetheless, we offer customization options for each dataset integrated in the loader method. For seamless integration, all datasets are fully compatible with **PYTORCH GEOMETRIC** through its `InMemoryDataset` interface. We provide **GRAPHBENCH** as a Python package distributed via PyPi under the name `graphbench-lib`, enabling continuous updates to code and datasets.

Beyond loading datasets, **GRAPHBENCH** provides utilities for experimentation. Given a model, hyperparameter optimization can be run directly via `graphbench.Optimizer`, which implements the optimization algorithms described in Section 5. For evaluation, `graphbench.Evaluator` loads the corresponding metrics for each selected dataset. Since specific datasets require specialized architectures (e.g., for graph generation), we also supply example architectures and usage guidelines in our code repository. Listing 1 presents pseudocode for training a predefined model using **GRAPHBENCH**.

```

1 import graphbench-lib as graphbench
2
3 model = #your torch model
4 dataset_name = #name of the task or list of tasks
5 pre_filter = #PyTorch Geometric filter matrix
6 pre_transform = #PyTorch Geometric-like transform during loading
7 transform = #PyTorch Geometric-like transform at computation time
8
9 #Setting up the components of graphbench
10 Evaluator = graphbench.Evaluator(dataset_name)
11 Optimizer = graphbench.Optimizer(optimization_args, training_method)
12 Loader = graphbench.Loader(dataset_name, pre_filter, pre_transform, transform)
13
14 #load a GraphBench dataset and get splits
15 dataset = Loader.load()
16
17 #optimize your model
18 opt_model = Optimizer.optimize()
19
20 #use graphbench evaluator with targets y_true and predictions y_pred
21 results = Evaluator.evaluate(y_true, y_pred)

```

Listing 1: **PYTORCH**-like pseudocode for **GRAPHBENCH** showcasing the usage of the dataset loader and application to downstream tasks.

¹See <https://github.com/graphbench/package> for the source code.

Table 2: Statistics of currently-available **GRAPHBENCH** datasets.

Category	Name	#Graphs	Avg. #Nodes	Avg. #Edges	Avg. Deg.
Social networks	BlueSky – quotes	1	289 136 / 286 425 / 311 272	3 075 967 / 3 815 996 / 4 525 872	10.64 / 13.32 / 14.54
	BlueSky – replies	1	470 816 / 464 867 / 569 424	9 287 565 / 10 769 386 / 12 318 196	19.73 / 23.17 / 21.63
	BlueSky – reposts	1	498 012 / 508 818 / 580 112	12 049 951 / 14 658 114 / 17 261 865	24.20 / 28.81 / 29.76
Chip design	AIG	1 200 000	125.9	236.3	3.7
Electronic circuits	5 Components	73 000	13.0	30.0	7.0
	7 Components	14 000	17.0	42.0	9.3
	10 Components	6 000	24.0	56.0	12.3
SAT Solving	Small – VG	69 596	1 323.96	38 791.52	33.9
	Small – VCG	69 596	8 304.22	45 402.51	5.4
	Small – LCG	69 596	9 628.12	45 402.05	4.75
Combinatorial optimization	RB – Small	50 000	241.0	9 016.1	36.9
	RB – Large	50 000	1 027.8	102 644.8	99.4
	ER – Small	50 000	249.9	9 463.5	37.3
	ER – Large	50 000	750.2	84 450.1	112.4
	BA – Small	50 000	249.9	991.6	3.9
	BA – Large	50 000	750.1	2 992.4	3.9
Algorithmic reasoning-EASY	Topological Sorting	1 020 000	16.0 / 16.0 / 128.0	41.006 / 40.997 / 1121.008	2.563 / 2.562 / 8.758
	MST	1 020 000	16.0 / 16.0 / 128.0	24.024 / 24.004 / 1147.972	1.5015 / 1.5003 / 8.9685
	Bridges	1 020 000	16.0 / 16.0 / 128.0	20.754 / 20.794 / 277.08	1.2971 / 1.2996 / 2.1647
	Steiner Trees	1 020 000	16.0 / 16.0 / 128.0	28.739 / 28.733 / 755.284	1.796 / 1.796 / 5.901
	Max Clique	1 020 000	16.0 / 16.0 / 128.0	77.99 / 77.95 / 2698.5	4.875 / 4.872 / 21.081
	Flow	1 020 000	16.0 / 16.0 / 64.0	75.76 / 75.84 / 530.96	4.734 / 4.740 / 8.296
	Max Matching	1 020 000	16.0 / 16.0 / 128.0	38.890 / 38.897 / 746.453	2.431 / 2.431 / 5.834
Algorithmic reasoning-MEDIUM	Topological Sorting	1 000 000	16.0 / 16.0 / 128.0	36.167 / 36.137 / 1097.05	2.260 / 2.259 / 8.571
	MST	1 020 000	16.0 / 16.0 / 128.0	23.976 / 24.003 / 1140.312	1.498 / 1.50 / 8.909
	Bridges	1 020 000	16.0 / 16.0 / 128.0	17.539 / 17.54 / 277.550	1.0962 / 1.0963 / 2.168
	Steiner Trees	1 020 000	16.0 / 16.0 / 128.0	19.549 / 19.562 / 742.301	1.222 / 1.223 / 5.799
	Max Clique	1 020 000	16.0 / 16.0 / 128.0	108.0 / 108.0 / 2 687.22	6.751 / 6.751 / 20.994
	Flow	1 020 000	16.0 / 16.0 / 64.0	42.36 / 42.36 / 645.20	2.648 / 2.648 / 10.08
	Max Matching	1 020 000	16.0 / 16.0 / 128.0	16.305 / 16.306 / 726.908	1.0189 / 1.020 / 5.679
Algorithmic reasoning-HARD	Topological Sorting	1 020 000	16.0 / 16.0 / 128.0	36.143 / 36.142 / 827.09	2.259 / 2.259 / 6.462
	MST	1 020 000	16.0 / 16.0 / 128.0	24.008 / 23.998 / 978.825	1.50 / 1.499 / 7.647
	Bridges	1 020 000	16.0 / 16.0 / 128.0	17.539 / 17.54 / 277.08	1.096 / 1.096 / 2.165
	Steiner Trees	1 020 000	16.0 / 16.0 / 128.0	19.583 / 19.565 / 663.547	1.224 / 1.223 / 5.184
	Max Clique	1 020 000	16.0 / 16.0 / 128.0	108.01 / 107.99 / 1812.04	6.751 / 6.750 / 14.157
	Flow	1 020 000	16.0 / 16.0 / 64.0	42.36 / 42.36 / 645.20	2.648 / 2.648 / 10.08
	Max Matching	1 020 000	16.0 / 16.0 / 128.0	16.303 / 16.304 / 746.521	1.018 / 1.019 / 5.832
Weather forecasting	ERA5 64x32	93 544	4 610	59 667	12.9

3. Overview of GraphBench’s datasets

In the following, we provide an overview of **GRAPHBENCH**’s domains and the provided datasets.

3.1. Social sciences

The social sciences domain in **GRAPHBENCH** includes datasets that model human interactions and societal processes as graphs, where nodes represent individuals or entities and edges represent relationships or communications. These graphs facilitate evaluation of tasks such as link prediction, community detection, and temporal forecasting, providing valuable insights into real-world social systems.

3.1.1. Social networks: Predicting engagements on BlueSky

Social networks—graphs with users as nodes and interactions as edges—provide a structurally rich domain for graph-based machine learning [Newman, 2010]. They exhibit hubs, peripheral nodes,

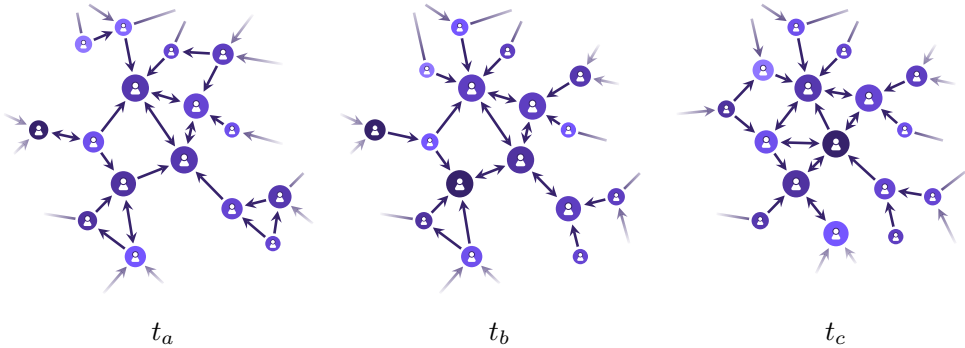


Figure 2: Excerpt of a dynamic social network over three timesteps $t_a < t_b < t_c$ constructed from the BlueSky dataset. Node features are displayed by color gradient, and the target value is encoded by node size. Edges may be rewired between timesteps.

clustered communities, and evolving, often directed edges. Dynamic user interests create temporal dependencies that shape representations and predictions. These properties make social networks valuable benchmarks for graph learning, requiring models to handle edge directionality and structural diversity. In particular, our proposed benchmark involves predicting the number of engagements a user will receive on upcoming posts, i.e., a user-centric measure of near-term influence, with applications in user ranking, trend detection, influencer marketing, and proactive moderation. Figure 2 provides an overview of how the graph is constructed from the BlueSky dataset and changes over time.

Related work A wide range of social network benchmarks are available in repositories such as SNAP [Leskovec and Sosic, 2016] and TUDATASETS [Morris et al., 2020], yet these datasets diverge substantially from real-world social networks. Benchmarks such as FACEBOOK, GITHUB, TWITCH, LASTFM, DEEZER, and REDDIT [Rozemberczki et al., 2021, Hamilton et al., 2017] illustrate the main issues: (1) interactions are collapsed into static graphs, eliminating temporal dynamics; (2) prediction targets are categorical (e.g., user type, demographic attribute) rather than continuous behavioral outcomes; (3) topologies are simplified to undirected friendships or follows, omitting richer relations such as replies, reposts, or pull requests; (4) node features are weak or outdated, often sparse indicators or embeddings from GloVe/Word2Vec; and (5) preprocessing alters network structure in disruptive and biasing manners, for example by removing large communities in REDDIT. The TUDATASET collection shares similar limitations. Their REDDIT variants represent discussion threads as featureless graphs with reply edges and categorical thread-level labels, while COLLAB and IMDB construct ego-networks labeled by field or genre. These datasets are likewise static, categorical, topologically restricted, feature-poor, and further constrained by artificial graph boundaries that remove long-range dependencies. Our datasets are designed to support more realistic forecasting, with temporally consistent splits, continuous engagement-based targets, and interaction topologies that preserve multiple directed relation types. Node features are derived from user-generated text using modern language-model embeddings, and networks do no undergo *arbitrary* subsampling.

Description of the learning task We cast the problem as node-wise regression to predict an aggregated statistic on the engagements a user will receive on their future posts. For any interval $\tau_{A,B} := (t_A, t_B] := \{t_A+1, \dots, t_B\}$ ², we define the following.

- **Interaction graph:** $G_{\tau_{A,B}}^\iota := (V, E_{\tau_{A,B}}^\iota)$ where V , the node set, consists of social network users, and $E_{\tau_{A,B}}^\iota \subseteq V \times V$ is the set of *directed* interactions of kind ι ($\iota \in \{\text{quotes, replies, reposts}\}$) observed in $\tau_{A,B}$.
- **Content:** $T_{\tau_{A,B}}^{(u)} := \{\mathbf{c}_{u,p_t} \mid t \in \tau_{A,B}\}$ collects the textual content for post p authored by user $u \in V$ at any $t \in \tau_{A,B}$ (i.e., \mathbf{c}_{u,p_t}).
- **Engagements:** $E_{\tau_{A,B}}^{\kappa,(u)} := \{e_{u,p_t}^\kappa \mid t \in \tau_{A,B}\}$ collects the number of engagements of kind $(\kappa, \kappa \in \{\text{likes, replies, reposts}\})$ received by posts p authored by u at $t \in (t_A, t_B]$. We define an aggregate statistic $y_{\tau_{A,B}}^{\kappa,(u)} = \mu(E_{\tau_{A,B}}^{\kappa,(u)})$.

Given timestamps $t_0 < t_1 < t_2$, user u and target engagement κ , the learning task is to predict value $y_{\tau_{1,2}}^{\kappa,(u)}$ given the overall interaction graph $G_{\tau_{0,1}}^\iota$ and post contents $\{T_{\tau_{0,1}}^{(u)} \mid u \in V\}$. We assess model performance using the mean absolute error (MAE), coefficient of determination R^2 , and the Spearman correlation σ , where the last two are calculated specifically for each target engagement κ . We note that σ is relevant to us since it measures how well predictions preserve the relative ordering of users by future engagements, a key criterion when ranking influence in heavy-tailed social networks, not necessarily captured by MAE and R^2 . See more on the evaluation metrics in Section A.1.

Details on the dataset We build upon the publicly available BLUESKY³ dataset curated by Failla and Rossetti [2024], referring the reader to their paper for full details on the data collection and curation process. In the following, we summarize the components relevant to our benchmark.

- *Graph structures.* The dataset contains three graph structures that capture network-wide *interactions* based on quotes, replies, and reposts: a *directed* edge from node u to node v indicates that u quoted, replied to, or reposted v . These interactions are originally timestamped and employ this information to construct graph structures temporally consistent with the proposed time-based splits, i.e., made up only of interactions in $\tau_{0,1} = (t_0, t_1]$. We only consider one single edge when multiple interactions are present in $\tau_{0,1}$ for the same user pair. In future iterations of this dataset, we will consider endowing edges with additional features conveying the amount and time distribution of such interactions.
- *Node features.* Each node corresponds to a user, which we describe with an aggregated representation of the content of their posts. For each user, we employ the SENTENCE-TRANSFORMERS/ALL-MiniLM-L6-v2 language model to embed the text obtained by concatenating the content of each of their posts at the monthly granularity.⁴ We subsequently aggregate these (by averaging) over the time interval $(t_0, t_1]$.
- *Node targets.* These are calculated as the *median* number of engagements obtained by the user's posts ($y_{\tau_{A,B}}^{\kappa,(u)} = \text{median}(E_{\tau_{A,B}}^{\kappa,(u)})$).⁵ These are considered as separate prediction targets and are

²In our setup, t 's represent discrete timesteps in seconds.

³<https://bsky.app/>

⁴<https://huggingface.co/sentence-transformers/all-MiniLM-L6-v2>

⁵We observed the median be a more robust statistic w.r.t., e.g., the mean, in this context.

measured in the time interval $(t_1, t_2]$. We apply a logarithmic transformation to reduce the skewness of these prediction targets.

- *Splitting procedure.* The splitting strategy ensures that models are trained exclusively on past information and evaluated on later interactions. The posts considered in the derivation of node features and targets span a time interval from t_{start} to t_{end} . On top of these, we consider three key time points: t_A , t_B , t_C . These are obtained in a way that the proportion of posts in $\tau_{\text{start},A}, \tau_{A,B}, \tau_{B,C}, \tau_{C,D}$ amounts to, resp., 55%, 15%, 15%, 15%. The dataset is then accordingly split into training, validation, and test splits as follows:

- Training: $t_0 = t_{\text{start}}, t_1 = t_A, t_2 = t_B$;
- Validation: $t_0 = t_{\text{start}}, t_1 = t_B, t_2 = t_C$;
- Test: $t_0 = t_{\text{start}}, t_1 = t_C, t_2 = t_{\text{end}}$.

While ensuring the model is not trained on post contents and network interactions from the future, by setting $t_0 = t_{\text{start}}$ in all splits this partitioning strategy also reflects a realistic scenario where a social network “grows in time,” in the sense that user representations evolve as they generate new content and their connections expand as they interact with more users. See Section A.1 for details on the exact values of $t_{\text{start}}, t_{\text{end}}, t_0, \dots, t_2$.

Experimental evaluation and baselines We assess model performance on three different interaction types: *quotes*, *replies*, *reposts* and for three different engagement types: *likes*, *replies*, and *reposts*. As for baselines in comparison, we included DeepSets [Zaheer et al., 2017], MLPs, and MPNNs. Note that the first two are connectivity-agnostic; unlike MLPs, DeepSets access, however, *global* feature information; see more in Section B.3.

Results Table 3 shows a clear, consistent ordering from DeepSets to MLPs to MPNNs, across all interaction types in terms of lower MAE, higher R^2 , and Spearman (σ). These results suggest that *local, directed relational structures* are informative for predicting engagements over a short time horizon, as both DeepSets and MLPs, which ignore graph structure, lag behind MPNNs. However, it has to be noted that the global feature information accessed by DeepSets appears detrimental. We also note that the absolute values of R^2 and σ remain relatively low, indicating that the proposed tasks are far from being solved and leaving room for meaningful gains through more advanced, task-specific MPNNs.

Experimental evaluation and baselines Table 3 shows a clear, consistent ordering from DeepSets to MLP to GNN, across all interaction types (quotes, replies, reposts) in terms of lower MAE, higher R^2 , and Spearman (σ). These results suggest that *local, directed relational structures* are informative for predicting engagements over a short time horizon, as both DeepSets and MLPs, which ignore graph structure, lag behind GNNs. Unlike MLPs, DeepSets consider *global* feature information across the entire network, which appears detrimental. We also note that the absolute values of R^2 and σ remain relatively low, indicating that the proposed tasks are far from being solved and leaving room for meaningful gains through more advanced, task-specific GNNs.

Table 3: **Social Networks.** Performance metrics for each model on the different datasets. Test MAE, R^2 , and Spearman correlation are reported.

Dataset	Model	MAE	R^2_{likes}	R^2_{replies}	R^2_{reposts}	σ_{likes}	σ_{replies}	σ_{reposts}
quotes	DeepSets	0.810 \pm 0.005	0.140 \pm 0.002	0.102 \pm 0.002	0.138 \pm 0.002	0.307 \pm 0.004	0.178 \pm 0.002	0.334 \pm 0.003
	GNN	0.768 \pm 0.002	0.165 \pm 0.002	0.134 \pm 0.002	0.175 \pm 0.002	0.330 \pm 0.003	0.192 \pm 0.002	0.337 \pm 0.022
	MLP	0.784 \pm 0.001	0.145 \pm 0.001	0.107 \pm 0.001	0.141 \pm 0.001	0.308 \pm 0.003	0.176 \pm 0.002	0.335 \pm 0.002
replies	DeepSets	0.789 \pm 0.033	0.086 \pm 0.033	0.061 \pm 0.024	0.104 \pm 0.014	0.253 \pm 0.003	0.130 \pm 0.001	0.240 \pm 0.006
	GNN	0.694 \pm 0.002	0.158 \pm 0.003	0.119 \pm 0.002	0.159 \pm 0.002	0.258 \pm 0.009	0.132 \pm 0.006	0.247 \pm 0.011
	MLP	0.725 \pm 0.004	0.131 \pm 0.003	0.087 \pm 0.003	0.122 \pm 0.003	0.249 \pm 0.004	0.127 \pm 0.005	0.243 \pm 0.003
reposts	DeepSets	0.918 \pm 0.013	0.049 \pm 0.005	0.031 \pm 0.012	0.050 \pm 0.009	0.229 \pm 0.004	0.129 \pm 0.007	0.205 \pm 0.009
	GNN	0.832 \pm 0.009	0.131 \pm 0.017	0.111 \pm 0.022	0.128 \pm 0.008	0.284 \pm 0.044	0.143 \pm 0.032	0.260 \pm 0.051
	MLP	0.874 \pm 0.003	0.087 \pm 0.002	0.051 \pm 0.003	0.066 \pm 0.002	0.234 \pm 0.008	0.123 \pm 0.006	0.206 \pm 0.010

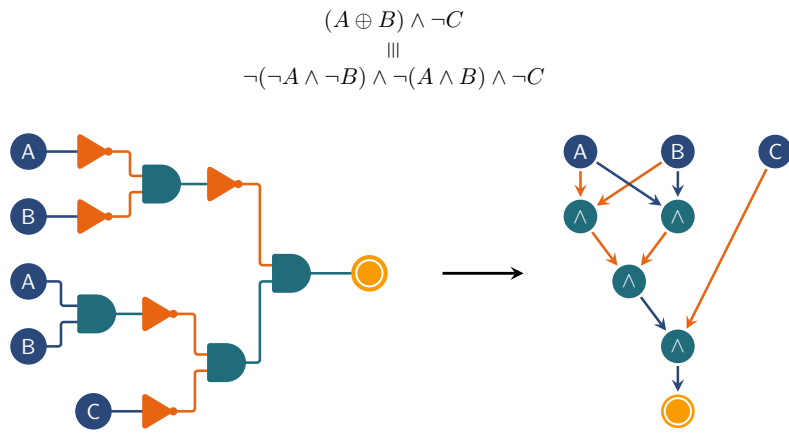


Figure 3: Transformation of a Boolean formula into an And–Inverter Graph (AIG). The left side shows the logic network with explicit gates and inversions; the right side shows the corresponding AIG representation using only AND nodes (teal) and negated edges (orange).

3.2. Hardware design

The hardware design domain in GRAPHBENCH encompasses datasets that represent electronic circuits as graphs, where nodes correspond to components such as transistors, resistors, or logic gates, and edges denote their (electrical) connections. These graphs are well-suited for evaluating models for tasks such as circuit optimization and performance prediction, which are critical for advancing efficient and reliable hardware development.

3.2.1. Chip design: Learning to generate small circuits

Chip design is among the most complex engineering challenges today, with significant implications for the global economy and supply chains [Ou et al., 2024]. Fabricating a competitive system-on-chip requires arranging billions of transistors under strict performance, power, and area constraints. This process is orchestrated by *electronic design automation* (EDA) tools, which automate key stages from high-level synthesis to physical layout. Yet, as design scale and complexity continue to grow,

bottlenecks in design space exploration and functional verification are becoming increasingly severe.

Logic synthesis is a fundamental step within the EDA flow, translating a behavioral specification into a structural implementation of interconnected logic gates [Rai et al., 2021]. The resulting Boolean circuit provides the core representation of a system’s logic. Optimizing this circuit, typically by minimizing its size (area), is a well-known NP-hard problem [Ilango et al., 2020]. For decades, progress has relied on carefully engineered heuristics and combinatorial optimization techniques embedded in EDA tools. However, these classical approaches are reaching diminishing returns, and their computational costs scale poorly with modern circuit complexity [Tsaras et al., 2025].

Recently, machine learning has begun to influence key stages of chip design, including macro placement [Mirhoseini et al., 2021] and floor planning [Mallappa et al., 2024]. In this work, we propose focusing these efforts on logic synthesis, framing it as a conditional graph generation problem: generating a circuit that correctly implements a given Boolean function while minimizing the number of gates. The goal is thus to produce circuits that satisfy a prescribed truth table exactly while optimizing structural efficiency.

A central challenge in Boolean circuit synthesis is ensuring optimized circuits remain functionally equivalent to the original. Regardless of transformations aimed at reducing gate count, delay, power, or area, outputs must match for all inputs. This makes the task delicate—small changes can alter behavior. Finding a minimal circuit is NP-hard, making synthesis a core computational challenge. Classical tools like ABC [Brayton and Mishchenko, 2010] use heuristics to generate near-optimal circuits efficiently. Recently, learning-based methods have emerged as alternatives [Mirhoseini et al., 2021, Li et al., 2025b], using data-driven models to capture structural patterns and generalize across designs. Boolean circuits’ natural representation as directed acyclic graphs makes graph-based generative learning particularly promising.

Formally, let $f: \{0,1\}^n \rightarrow \{0,1\}^m$ be a Boolean function with n inputs and m outputs. Its behavior is fully specified by a truth table $\mathbf{T}^f \in \{0,1\}^{m \times 2^n}$, where each column \mathbf{T}_x^f corresponds to an input $x \in \{0,1\}^n$ and satisfies $f(x) = \mathbf{T}_x^f$. A logic circuit $C := (V, E)$ is represented as a *directed acyclic graph* (DAG) of in-degree at most two. The node set is partitioned into input nodes $V^{\text{in}} := \{v_1^{\text{in}}, \dots, v_n^{\text{in}}\}$, gate nodes $V^{\text{gate}} := \{v_1^{\text{gate}}, \dots, v_k^{\text{gate}}\}$, each computing a Boolean function of arity at most two (e.g., AND), and output nodes $V^{\text{out}} := \{v_1^{\text{out}}, \dots, v_m^{\text{out}}\}$, each of in-degree one. The edge set $E \subseteq V \times V \times \{0,1\}$ specifies connections, where a label of 1 denotes signal inversion (Not) and 0 denotes direct transmission. For an input $x \in \{0,1\}^n$, values are assigned to input nodes, propagated through gate nodes (applying inversion where specified), and collected at output nodes to yield the circuit output $C(x) \in \{0,1\}^m$. Because the combination of AND and Not is functionally complete, any Boolean function can be represented using only these two operations. We therefore adopt the standard representation of *and-inverter graphs* (AIGs), where circuits are DAGs of AND gates connected by edges that may invert their signals [Mishchenko et al., 2005]. AIGs are widely used in industrial logic synthesis and provide a compact, canonical representation of circuits. Figure 3 provides an overview of how the AIG is constructed from a Boolean formula and how it compares to traditional logic gates.

Related work AlphaChip [Mirhoseini et al., 2021] kickstarted efforts to bring the latest machine learning advancements into a relatively conservative area of chip design, applying reinforcement learning to the macro placement task and outperforming human engineers on specific metrics, as well as processing designs for newer generations of TPUs [Goldie et al., 2024]. In logic synthesis, considerable work has focused on discriminative objectives [Zheng et al., 2025] rather than generative

ones. One of the main benchmarks in the field is the contest organized by the *International Workshop on Logic & Synthesis* (IWLS) [Mishchenko and Miyasaka, 2023] where participants are asked to optimize 100 pre-selected circuits. Historically, combinatorial optimization methods prevailed due to the lack of training splits and the limited amount of available data. However, recent machine learning methods have shown promising results by training on large amounts of synthetic data simulated with standard EDA tools.

Description of the learning task Given a set of N Boolean functions, $\{f_i\}_{i=1}^N, N \in \mathbb{N}, f_i: \{0, 1\}^{n_i} \rightarrow \{0, 1\}^{m_i}$, the goal of Boolean circuit synthesis is to construct, for each function, a logic circuit $C_i = (V_i, E_i)$ with n_i input and m_i output nodes that satisfies the following conditions.

1. **Logical correctness (constraint)** For all $x \in \{0, 1\}^{n_i}$, the output of the circuit must match the output of f_i , i.e., $C_i(x) = f_i(x)$, where $C_i(x)$ denotes the vector of output values produced by the circuit on input x . In that case, C_i is said to be *logically equivalent* to f_i , which we denote $C_i \equiv f_i$.
2. **Structural efficiency (objective)** For each f_i , among all circuits $C = (V, E)$ satisfying logical correctness, select a circuit that optimizes a predefined circuit score function $s(C)$, where $s: C_{f_i} \rightarrow \mathbb{R}_{\geq 0}$, which measures structural properties of the circuit, such as the number of gate nodes,

$$\arg \max_{C \in C_{f_i}} s(C),$$

where $C_{f_i} = \{C \mid C \equiv f_i\}$ is the set of all circuits implementing f_i . The score function should favor AIGs with fewer internal nodes while penalizing incorrect solutions. Therefore, we define score over the set of functions $\{f_i\}_{i=1}^N$ as

$$\text{score}(\tilde{C}) := \frac{100}{N} \sum_{i=1}^N \frac{\#C_i^{\text{ref}}}{\#\tilde{C}_i} \cdot \mathbb{1}_{\tilde{C}_i \equiv f_i}, \quad (1)$$

where \tilde{C} is the set of generated AIGs, $\#\tilde{C}_i$ and $\#C_i^{\text{ref}}$ are the number of internal nodes of the i -th generated circuit and of the corresponding baseline AIG generated by ABC, $\mathbb{1}_{\tilde{C}_i \equiv f_i} = 1$ if \tilde{C}_i is logically equivalent to f_i , and 0 otherwise.

With this benchmark, we introduce a new generative task paired with a challenging optimization objective, i.e., models must generate valid tree-like DAGs that not only satisfy a target truth table but also minimize circuit size. This setting provides a rigorous testbed for evaluating the capabilities of generative graph methods under realistic and computationally challenging constraints.

Details on the dataset For this benchmark, we require paired datasets of truth tables and their corresponding AIGs to train generative models. To construct such a dataset, we first generated 1 200 000 random truth tables in the PLA format [Wille et al., 2008], each with 6-8 inputs and 1 or 2 outputs. These truth tables were then compiled into optimized AIGs in the AIGER format [Biere et al., 2011] using ABC. During this step, we applied a sequence of standard optimization commands (`strash`, `resyn2`, `resyn2`, `dc2`, `resyn2rs`, `resyn2`). We subsequently converted the AIGs into DOT format [Gansner et al., 2006] via the AIGER library, from which they can be conveniently transformed into PYTORCH GEOMETRIC graphs. Alongside these graph representations, we store the truth tables explicitly as matrices of size $m \times 2^n$, where n is the number of inputs and m the number

of outputs. We split the dataset into train, validation, and test sets using an 80/10/10 split. Details concerning the dataset are presented in Table 4.

Table 4: Statistics of the synthetic AIG dataset.

#Graphs	#Inputs	#Outputs	Mean #Nodes	Median #Nodes	Max. #Nodes
1.2M	6-8	1-2	125.9	104.0	335.0

Experimental evaluation and baselines We report results using four standard ABC variants.

- STRASH converts the circuit into an AIG representation using structural hashing. This serves as the basis for subsequent optimizations.
- RESYN is a lightweight synthesis script that alternates between balancing and rewriting.
- COMPRESS2 applies balancing, rewriting, and refactoring, together with zero-cost replacements, to restructure the network and enable further simplifications.
- RESYN2RS is a heavyweight optimization script that performs multiple rounds of balancing, rewriting, refactoring, and resubstitution, progressively increasing the cut sizes ($K = 6$ to 12).

As you may notice, the methods are ordered by complexity, with STRASH being the simplest and lightest, and RESYN2RS the most complex and expensive. Notably, we do not include any learning-based baselines for this dataset. While numerous graph-generative approaches exist (e.g., Vignac et al. [2023]), most are designed for undirected graphs and thus unsuitable for DAGs. Moreover, our experiments with two DAG-specific generative methods, LayerDAG [Li et al., 2025a] and Directo [Carballo-Castro et al., 2025], indicate that they fail to produce circuits functionally equivalent to the target truth table. This suggests a new and unexplored direction for the graph generation community, i.e., developing conditional DAG generative models that enforce strict constraints, such as functional equivalence with a given truth table.

Results Our results using four different ABC variants are reported in Table 5. We report the score defined in Equation (1). The methods rank consistently with their complexity across all settings, with the simple STRASH yielding the worst results and the advanced RESYN2RS achieving the best performance.

Table 5: **Chip Design.** Results of the different ABC methods on the AIG dataset. Higher is better.

Method	Number of (inputs, outputs)						
	(6,1)	(6,2)	(7,1)	(7,2)	(8,1)	(8,2)	Overall
STRASH	73.90	74.23	76.55	75.71	77.63	76.52	75.76
RESYN	86.79	88.16	89.28	89.05	90.45	89.78	88.92
COMPRESS2	92.53	93.57	93.18	92.79	93.28	92.49	92.97
RESYN2RS	93.30	95.24	95.15	95.64	96.24	96.11	95.28

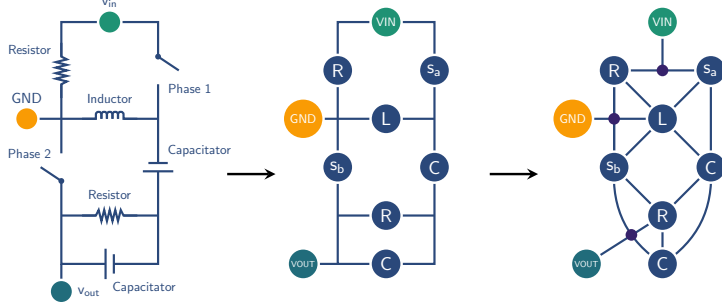


Figure 4: Transformation of an electronic circuit into a graph.

3.2.2. Electronic circuits: Predicting voltage conversion ratio

Analog circuit design remains critical but labor-intensive in EDA [Zhang et al., 2019, 2020, Zhao and Zhang, 2020]. Unlike mature digital flows, analog design still relies on expert intuition due to sensitivity to device variations and complex constraints. This is especially true for custom power-converter design, where topology generation and parameter tuning must balance conflicting metrics. Even with a modest number of components, hundreds of thousands of topologies are possible; yet, new converter families are mostly handcrafted. Automating this process could accelerate design cycles and expand the exploration of novel architectures. Learning-based methods offer promise as surrogate models that predict performance [Fan et al., 2021, 2024b], enabling faster search over vast spaces. Power converters’ natural graph structure makes them an ideal benchmark, highlighting robustness to structural sensitivity and the ability to cope with extreme class imbalance. Figure 4 provides an overview of how an electronic circuit is transformed into a graph.

Related work Learning for circuit design has been explored for physical implementation [Lu et al., 2020] and parameter optimization [Wang et al., 2020], typically under the assumption of fixed topologies. Topology exploration, in contrast, has relied on heuristic search, including evolutionary and genetic algorithms [McConaghay et al., 2011], as well as tree-based strategies [Fan et al., 2021, Zhao and Zhang, 2020]. Our benchmark differs by treating performance prediction as a supervised graph learning task, using standardized splits and metrics to enable systematic comparison across architectures.

Description of the learning task Each circuit is represented as a graph $G = (V, E)$. The node set V contains device components: capacitors (C), inductors (L), and two phase-specific switches (S_a, S_b), and three external terminal ports: input (V_{in}), output (V_{out}) and ground (GND). Each component node $v \in V$ has a type $\tau(v)$ and (optional) parameter vector d_v and connects to other devices or ports via exactly two edges; each terminal node has a single outgoing edge. Edges E denote electrical interconnections between ports. Given a graph G , encoding a power converter, the prediction task is to estimate two continuous performance metrics: (1) the *voltage conversion ratio* (output-to-input voltage) and (2) the *power conversion efficiency* (fraction of input power delivered to the load). Performance is evaluated via the *relative squared error*, reported separately for each target,

$$RSE(y, \hat{y}) := \frac{\sum_{i=1}^N (y_i - \hat{y}_i)^2}{\sum_{i=1}^N (y_i - \bar{y})^2}, \quad (2)$$

where y_i is the ground-truth value from high-fidelity simulation, \hat{y}_i the model prediction, \bar{y} the mean of $\{y_i\}_{i=1}^N$, and N the number of evaluation samples.

Details on the datasets Following the setting proposed by Fan et al. [2024b], we used datasets at three complexity levels, generated from random valid topologies with 5, 7, and 10 components. Topologies are sampled uniformly at random under connectivity constraints; isomorphic copies are removed to ensure uniqueness. Each instance is simulated with NGSPICE [Nenzi and Vogt, 2011] to obtain ground-truth voltage conversion ratio and efficiency; instances flagged as invalid during simulation are discarded. Unless otherwise specified, component and operating parameters are fixed as follows: capacitors $10 \mu\text{F}$, inductors $100 \mu\text{H}$, input voltage 100 V , switching frequency 1 MHz , an input resistor of 0.1Ω at V_{in} , and a 100Ω load with a $10 \mu\text{F}$ output capacitor at V_{out} . The resulting datasets contain approximately 73k, 14k, and 6k instances for the 5-, 7-, and 10-component settings, respectively. Graphs typically comprise more than 13 internal nodes (plus three terminals) for 5-component circuits, and over 17 and 24 internal nodes for the 7- and 10-component sets, respectively.

Experimental evaluation and baselines We evaluate four standard methods, including the GT and MPNN-based models (see Table 6), using the score defined in Equation (2). Experiments are conducted on datasets containing 5, 7, and 10-component circuits. For each dataset, models are trained from scratch and evaluated on circuits of the same size. Table 6 reports the relative squared error (RSE) for efficiency and output voltage prediction, comparing the GT with baseline models (GCN, GAT, and GIN) as circuit complexity increases. Results confirm that the GT consistently achieves higher prediction accuracy than baseline models, not only on smaller circuits but also across datasets with varying circuit sizes and prediction targets. The rise in RSE for larger circuits is mainly due to the reduced availability of training data from costly high-fidelity simulations, combined with the combinatorial growth of circuit space, which makes learning increasingly difficult for all models.

Results We conduct experiments on datasets containing 7- and 10-component circuits, extending beyond the 5-component dataset. In each experiment, a model is trained from scratch and evaluated on a dataset containing circuits of the same size. Table 6 presents the RSEs for efficiency and output voltage prediction, comparing GT with baseline models (GCN, GAT, and GIN) as circuit size increases.

3.3. Reasoning and optimization

This GRAPHBENCH domain targets graph learning tasks involving complex reasoning and hard optimization, from theorem proving and hardware verification to logistics and network design. Models must capture fine-grained structural dependencies and generalize across instances. We highlight three problem families: (i) *SAT solver selection and performance prediction*, which forecasts solver behavior or picks the best solver per instance; (ii) *combinatorial optimization*, including NP-hard problems like maximum independent set, max-cut, and graph coloring; and (iii) *algorithmic reasoning*, where models approximate outputs of polynomial-time graph algorithms. Benchmarks evaluate predictive accuracy, robustness, scalability, and (out-of-distribution) generalization.

Table 6: Performance comparison of baseline models on circuit datasets with 5, 7, and 10 components (RSE).

Task	Method	Size		
		5 comp	7 comp	10 comp
Efficiency	GT	0.07 \pm 0.03	0.18 \pm 0.06	0.29 \pm 0.03
	GIN	0.09 \pm 0.06	0.21 \pm 0.04	0.44 \pm 0.13
	GAT	0.11 \pm 0.05	0.22 \pm 0.05	0.38 \pm 0.05
	GCN	0.13 \pm 0.07	0.30 \pm 0.04	0.53 \pm 0.06
Voltage	GT	0.12 \pm 0.02	0.31 \pm 0.05	0.39 \pm 0.05
	GIN	0.14 \pm 0.05	0.35 \pm 0.03	0.54 \pm 0.12
	GAT	0.17 \pm 0.13	0.34 \pm 0.12	0.48 \pm 0.02
	GCN	0.18 \pm 0.07	0.46 \pm 0.08	0.61 \pm 0.07

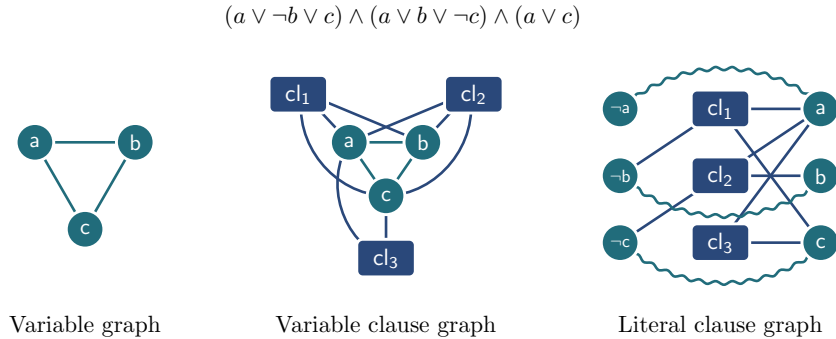


Figure 5: Overview of the three graph types generated from a given SAT formula.

3.3.1. SAT solving: Algorithm selection and performance prediction

The *Boolean satisfiability problem* (SAT) is a central and longstanding NP-complete problem [Karp, 1972, Biere et al., 2021]. It asks whether there exists a truth assignment that satisfies a Boolean formula φ over variables v_1, \dots, v_r , typically expressed in *conjunctive normal form* (CNF):

$$\varphi = \bigwedge_{i=1}^n c_i, \quad \text{where each } c_i = \bigvee_{j=1}^{m_i} l_{i,j}.$$

Here, each $l_{i,j}$ is a literal, i.e., either a variable v_p or its negation $\neg v_p$. The task is to decide whether there exists an assignment a such that $\varphi(a) = \text{true}$. SAT is of significant theoretical importance as one of the first problems proven NP-complete [Cook, 1971], and it underpins numerous practical applications in hardware and software verification [Biere et al., 2009], automated planning [Kautz and Selman, 1996], and operations research [Gomes et al., 2008]. Its significance has led to the development of a wide range of solvers, systematically benchmarked in annual SAT competitions (e.g., [Froleyks et al., 2021, Balyo et al., 2017, Heule et al., 2019]). A key property of modern SAT solvers is *performance complementarity*—no single solver dominates across all instances. This

motivates the study of *algorithm selection* [Rice, 1976, Xu et al., 2008], where the aim is to choose the most effective solver for a given instance. *Empirical performance prediction* is a closely related problem, which seeks to forecast the computation time (or another performance metric) of a solver on a given instance. Such predictions can support algorithm selection, configuration, scheduling, and explainability [Hutter et al., 2014a]. State-of-the-art methods for algorithm selection and performance prediction rely on *hand-crafted features* extracted from SAT instances. The most widely adopted feature set is that of the SATZILLA family of algorithm selectors [Nudelman et al., 2004, Hutter et al., 2014a, Shavit and Hoos, 2024]. These features include basic structural properties (e.g., number of clauses and variables), graph-based descriptors derived from instance structure, and probing features obtained by briefly running a solver to collect computation-time statistics. Machine learning models—most often tabular models—are then trained on these features for prediction or selection tasks.

SAT instances can be naturally represented as graphs, reflecting their permutation-invariant structure that arises from the commutativity and associativity of logical conjunction and disjunction. Indeed, many of the hand-crafted SATZILLA features are derived from such graph representations, including the

- *Variable-clause graph*: a bipartite, undirected graph with a node for each variable v and each clause c , where an edge connects a variable to a clause if and only if the variable appears in that clause.
- *Variable graph*: an undirected graph with one node per variable, where two variables v_i and v_j are connected if they co-occur in at least one clause.
- *Clause graph*: an undirected graph with one node per clause, where two clauses c_i and c_j are connected if they share at least one negated literal.

SATZILLA extracts statistical properties of these graphs—such as mean degree, coefficient of variation, clustering coefficient, and graph diameter—and uses them as features for downstream learning tasks.

Several studies have explored the use of GNNs or MPNNs to predict the satisfiability of a formula, e.g., Selsam et al. [2019]. Some of this work employs an additional representation, the *literal-clause graph*, a bipartite graph with one node per literal (a variable or its negation) and one node per clause, with edges linking literals to the clauses they appear in. However, many such approaches are *unsound*—they can produce incorrect results—or cannot guarantee valid satisfying assignments or proofs of unsatisfiability, limiting their practical usefulness [Selsam et al., 2019, Li et al., 2024c]. Other research has integrated MPNNs into existing SAT solvers to replace or guide solver heuristics [Wang et al., 2024, Tönshoff and Grohe, 2025]. These approaches retain the soundness and completeness guarantees of classical solvers while potentially accelerating the solving process. Nonetheless, benchmarking novel MPNN architectures in this setting is challenging, as it requires extensive pretraining and large-scale evaluations. A complementary line of work applies MPNNs to algorithm selection in SAT [Zhang et al., 2024, Shavit, 2023], predicting the most effective solver for a given instance directly from graph-based representations.

In GRAPHBENCH, we introduce, to the best of our knowledge, the largest algorithm-selection benchmark for SAT solvers, covering eleven solvers and more than 100 000 instances. Our benchmark supports multiple graph representations of SAT formulae and also provides the SATZILLA 2024 feature set [Shavit and Hoos, 2024], enabling their combination with MPNNs. Unlike existing GNN benchmarks for SAT [Li et al., 2024c], which primarily focus on satisfiability prediction or assignment

generation, our benchmark is designed for practical downstream tasks in SAT solving—specifically, algorithm selection and performance prediction. Figure 5 provides an overview of how the three graph types are constructed from a given Boolean formula.

Related work As the use of MPNNs for algorithm selection is a relatively new research direction, no benchmarks exist for this task. Previously, Shavit [2023] used a dataset of 3 000 synthetically generated SAT instances, while Zhang et al. [2024] used a proprietary dataset as well as the 2022 Anniversary track of the SAT Competition, while removing large instances. Outside of the graph domain, the ASLIB benchmark suite is used to benchmark algorithm selection methods [Bischl et al., 2016]. ASLIB contains multiple algorithm selection datasets from various domains, including SAT and TSP. Each dataset contains features extracted from the instances (such as SATZILLA) as well as the computation time of several algorithms on the instances. We note that ASLIB provides SAT scenarios based on a subset of SAT competitions, including instances and solvers from specific years. In contrast, our dataset comprises all available SAT competition instances, as well as numerous instances from other sources.

Description of the learning task We introduce two learning tasks. *Performance prediction* is a regression problem whose goal is to predict the computation time of SAT solvers on unseen instances, arising in applications such as algorithm selection [Rice, 1976] and algorithm configuration [e.g. Lindauer et al., 2022]. *Algorithm selection* is a multi-class classification problem that aims to select the best algorithm for a given instance. While algorithm selection can be reduced to performance prediction by choosing the solver with the lowest predicted computation time, we treat them as distinct problems. For algorithm selection, we adopt the loss function proposed by [Zhang et al., 2024], which penalizes the predicted probabilities in proportion to the solver’s computation time. Intuitively, a solver that only slightly underperforms on an instance incurs a small penalty, while poor selections are penalized more heavily, i.e.,

$$\frac{1}{N} \sum_{i=1}^N \left(\sum_{k=1}^K p_i^k \cdot t_i^k - t_i^* \right)^2,$$

where p_i^k is the predicted probability of selecting solver k for instance i , t_i^k is the computation time of solver k on instance i , and $t_i^* = \min_k t_i^k$ is the computation time of the *virtual best solver* (VBS). Each instance is provided with three graph-based representations VG, VCG, and LCG, described above. In all cases, SATZILLA features can be integrated as node attributes to enrich the graph representation.

The performance of a solver s on an instance set $\Pi = \{\pi_1, \pi_2, \dots, \pi_n\}$ is measured using the widely adopted *penalized average computation time* (PAR $_k$) metric, where k denotes the penalty factor for unsolved instances under a cutoff time c . The PAR $_k(s, \Pi)$ score is defined as the mean computation time of s across Π , where each unsolved instance contributes a computation time of $k \cdot c$. Lower PAR $_k$ values indicate better performance. For algorithm selectors, both feature extraction and model inference time are included in the total solving time, implying that MPNN inference must be efficient to be practically helpful.

For the performance prediction task, the model output is the base-10 logarithm of the PAR $_{10}$ score of solver s ,

$$\log_{10}(\text{PAR}_{10}(s, \Pi)),$$

a transformation shown to improve predictive accuracy in prior work [Hutter et al., 2014a]. Model performance is evaluated using the *root mean squared error* (RMSE) between predicted and actual

log-scaled computation times.

For algorithm selection, we use the *closed gap* (CG) metric, which quantifies how close a selector comes to the performance of the VBS relative to the single best solver (SBS). Formally,

$$\text{CG}(\Pi) = \frac{\text{PAR}_{10}(\text{SBS}, \Pi) - \text{PAR}_{10}(s, \Pi)}{\text{PAR}_{10}(\text{SBS}, \Pi) - \text{PAR}_{10}(\text{VBS}, \Pi)}.$$

A higher CG score indicates stronger selection performance, with CG = 1 corresponding to VBS performance and CG = 0 to SBS performance.

Details on the datasets We created the largest algorithm-selection scenario for SAT solvers to date. We collected all SAT Competition instances via GBD [Iser and Jabs, 2024] and added all instances from the AClab benchmark for algorithm configuration [Hutter et al., 2014b]. Together, these sources include SAT formulae from diverse real-world applications and synthetically generated instances. To further enrich the dataset, we generated additional formulae using three well-established SAT instance generators, i.e.,

- *FuzzSAT* [Brummayer et al., 2010] produces CNF fuzzing instances originally designed to identify issues in digital circuits. It generates random Boolean circuits as DAGs and converts them into CNF via the Tseitin transformation [Tseitin, 1983]. To construct the DAG, we used $v \in [50, 150]$ input variables; operands were randomly paired and connected by randomly chosen operator nodes until each input was referenced at least $t \in [1, 5]$ times. Finally, random clauses of length $s \in [3, 8]$ were added to increase complexity.
- *Cryptography* [Nejati et al., 2017, Alamgir et al., 2024] generates SAT instances encoding preimage attacks on MD4, SHA-1, and SHA-256. Each encoding applies multiple *rounds* of operations; higher numbers of rounds yield harder instances. We set the number of rounds to $d \in [16, 30]$, which produces formulae challenging for modern solvers but not unsolvable. Additionally, we fixed $i \in [0, 384]$ of the 512 input bits; fixing more bits results in easier instances.
- *Community attachment* [Giráldez-Cru and Levy, 2016] produces pseudo-random SAT formulae with community structure, a property often observed in real-world SAT encodings (e.g., hardware and software verification tasks [Ansótegui et al., 2012]). The generator can create relatively small but difficult instances. We used $n \in [1000, 3000]$ variables, $c \in [5, 100]$ communities, a clause-to-variable ratio of $[3.7, 4.5]$, and modularity factor $q \in [0.3, 0.9]$. Higher modularity values enforce stronger community structure.

For each generator, parameter ranges were chosen to yield challenging but still solvable instances. To ensure this, we excluded ranges of values yielding no instances solvable by KISSAT, the winner of the 2024 SAT Competition, between 1 and 5 000 seconds. After generation, we applied the SATELITE preprocessor to remove redundant clauses and variables. A summary of all generated instances is provided in Table 7.

We pre-selected solvers for the benchmark by constructing a portfolio of m complementary state-of-the-art SAT solvers, based on the results of the 2024 SAT Competition. Portfolios were built using beam search to identify the set of m solvers achieving the VBS performance. To determine m , we evaluated portfolios of all possible sizes and plotted portfolio size against achieved VBS. We then identified the inflection point (the “knee”) of this curve using the Kneedle algorithm [Satopaa et al., 2011] and adopted the corresponding portfolio. The ASF library [Shavit and Hoos, in progress] was

Table 7: Overview of the instances for the SAT solving benchmark.

Source	# of Instances	# of Variables			# of Clauses			
		min	max	avg	median	min	max	avg
SAT Competition	31 024	3	25 870 369	69 190.77	13 168.50	7	871 935 536	1 022 025.50
Community Attachment	29 994	922	2 956	1 931.05	1 928.00	3 566	13 413	8 088.71
AClib	33 955	6	248 738	3 319.65	1 270.00	24	103 670 100	136 471.03
FuzzSAT	8 020	2	944 685	10 217.75	1 820.00	1	4 094 516	45 638.30
Cryptography	4 873	6	12 415	4 264.89	3 225.00	24	185 006	55 309.63
Total	107 866	2	25 870 369	22 434.71	1 879.00	1	871 935 536	345 051.72
								10 177.50

used to perform the selection procedure. The same procedure was repeated on the SAT Competition 2023.

In total, our dataset includes the following solvers. From the 2024 SAT Competition: Kissat [Biere et al., 2024], BreadIdKissat [Bogaerts et al., 2024], AMSAT [Li et al., 2024b], and KissatMABDC [Liu et al., 2024]. From the 2023 SAT Competition: SBVA CadiCal [Haberlandt and Green, 2023], Reencode Kissat [Reeves and Bryant, 2023], Minisat XOR, KissatMAB Prop PR [Gao, 2023], hKissatInc [Tchinda and Djamegni, 2023], CadiCal vivinst [Biere et al., 2023], and BreakID Kissat [Bogaerts et al., 2023]. Solver computation times were measured in terms of CPU time using `runsolver` [Roussel, 2011] and the generic wrapper tools [Eggensperger et al., 2019], ensuring accurate and consistent performance measurement.

We provide three datasets, **SMALL**, which includes only small formulae with up to 3 000 variables and 15 000 clauses, **MEDIUM**, which consists of the small formulae with additional medium size formulae with size of up to 20 000 variables and 80 000 clauses and **LARGE**, which includes all formulae. This way, we provide datasets with varying hardness levels, as the size of the formula can pose hurdles for training time and GPU memory. While the **LARGE** and **MEDIUM** datasets are unlikely to be accessible on current hardware, we provide them to keep the benchmark relevant in the long term.

Experimental evaluation and baselines All SAT solving tasks in the benchmark are graph-level. For the graph transformer baselines, we employ an encoder-processor-decoder pipeline, as described in Section B, with no edge or node encoding. While we considered GT for the tasks, we encountered high computational costs in calculating the positional embeddings (more than a CPU day) and therefore excluded them from the evaluation. Furthermore, when training on medium- and large-sized graphs, we encountered out-of-memory errors even on an H100 with mixed-precision training. Consequently, we only consider small formulae for MPNNs. Similarly, we observed out-of-memory with the clause graphs, and therefore excluded them from the evaluation.

We note that traditionally, algorithm selection datasets are evaluated using cross-validation, primarily due to limited data availability. In contrast, our new dataset contains tens of thousands of formulas. Since it is also intended for deep learning approaches, which are computationally expensive and thus impractical to evaluate using 10-fold cross-validation, we instead provide a fixed train-validation-test split and report results across multiple random seeds.

For the performance prediction task, we compare the MPNNs against traditional baselines, which use the SATZILLA features and a (tabular) machine learning model. We use random forest [Breiman, 2001] and XGBoost [Chen and Guestrin, 2016], which are commonly used as empirical performance models (EPM) (see, e.g., Bansal et al. [2022], Eggensperger et al. [2015], Hutter et al. [2014c]). We use the SATZILLA 2024 features as input and predict the log10-scaled computation time. These

baselines are implemented using the ASF framework [Shavit and Hoos, in progress]. For algorithm selection, we provide several well-known baselines. First, we use pairwise regression [Kerschke et al., 2018] (PR; predicts performance differences between each pair of solvers, then picks the solver with the best sum), pairwise classification [Xu et al., 2012] (PC; predicts the better solver in each pair, then uses majority vote, winner of the ICON challenge on algorithm selection [Lindauer et al., 2019]) as well as a simple multi-class classification [Kotthoff, 2013] (MC; directly predicts the best solver). Similar to the EPM baselines, these baselines use the SATZILLA 2024 features with a random forest.

We furthermore considered AutoFolio [Lindauer et al., 2015] as a baseline. However, the smallest dataset we introduce contains more than 60 000 samples, whereas typical algorithm selection datasets (e.g., those in ASlib [Bischl et al., 2016]) have only hundreds to thousands of instances. As a result, AutoFolio failed to provide meaningful results and consistently predicted the single best solver. Additionally, the winner of the 2017 Open Algorithm Selection Challenge [Lindauer et al., 2019], ASAP [Gonard et al., 2017], lacks support for setting the pseudo-random seed and only allows cross-validation evaluation; therefore, we excluded it.

Table 8: **SAT Solving.** RMSE (\log_{10} time) for performance prediction on **small** SAT instances.

We report results on three different graph representations (VG, VCG, LCG) and using the hand-crafted SATzilla features. Lower is better.

Solver	Method	VG	VCG	LCG	SATZILLA
KISSAT	GIN	1.36 \pm 0.15	1.15 \pm 0.03	1.49 \pm 0.02	–
	RF	–	–	–	0.61 \pm 0.00
	XGB	–	–	–	0.63 \pm 0.00
BREAKIDKISSAT	GIN	1.29 \pm 0.03	1.33 \pm 0.15	1.52 \pm 0.01	–
	RF	–	–	–	0.65 \pm 0.00
	XGB	–	–	–	0.68 \pm 0.01
KISSATMABDC	GIN	1.27 \pm 0.00	1.43 \pm 0.24	1.60 \pm 0.01	–
	RF	–	–	–	0.70 \pm 0.00
	XGB	–	–	–	0.74 \pm 0.00
AMSAT	GIN	1.43 \pm 0.01	1.45 \pm 0.09	1.54 \pm 0.00	–
	RF	–	–	–	0.68 \pm 0.00
	XGB	–	–	–	0.72 \pm 0.01

Results We start by presenting the results for the performance prediction task. We present the RMSE of the log-scaled computation time for the solvers from SAT Competition 2024 (KISSAT, BREAKIDKISSAT, KISSATMABDC, AMSAT) for the small formulae in table Table 8. The table shows that traditional empirical performance predictors (random forest and XGBoost) that use hand-crafted features outperform MPNNs by a high margin. Furthermore, we observe significant differences between the various graph types. While usage of LCG is common as an input for MPNNs in the context of SAT solving [Selsam et al., 2019, Tönshoff and Grohe, 2025], the smaller VCG and VG perform better, which shows that the choice of input graph can have a strong influence on the results. We furthermore present the results of random forest and XGBoost on medium-size and large formulae in Tables 9a and 9b, such that they can be compared against graph machine learning solutions in the future. Overall, we observe that the random forest is the best-performing EPM for SAT solvers. For the algorithm selection task, we report the closed gap metric of different selectors in Table 10. The VG representation allows for better performance than Both VCG and LCG, although using GIN

Table 9: **SAT Solving.** RMSE (\log_{10} time) for performance prediction on MEDIUM and LARGE SAT instances. Lower is better.

(a) Medium-size SAT instances			(b) Large SAT instances		
Solver	Method	SATZILLA	Solver	Method	SATZILLA
KISSAT	RF	0.59 \pm 0.00	KISSAT	RF	0.58 \pm 0.00
	XGB	0.62 \pm 0.00		XGB	0.63 \pm 0.00
BREAKIDKISSAT	RF	0.64 \pm 0.00	BREAKIDKISSAT	RF	0.62 \pm 0.00
	XGB	0.67 \pm 0.00		XGB	0.67 \pm 0.00
KISSATMABDC	RF	0.68 \pm 0.00	KISSATMABDC	RF	0.66 \pm 0.00
	XGB	0.72 \pm 0.00		XGB	0.70 \pm 0.00
AMSAT	RF	0.64 \pm 0.00	AMSAT	RF	0.62 \pm 0.00
	XGB	0.67 \pm 0.00		XGB	0.66 \pm 0.00

across all three graph representation approaches, underperform pairwise regression with hand-crafted features. Furthermore, VG also outperforms multi-class classification and achieves a slightly smaller gap closure than pairwise classification. In contrast, using LCG leads to worse performance than the single best solver, indicating poor generalization to unseen instances. In their work, Zhang et al. [2024] claimed that their MPNN-based method outperforms traditional approaches. However, there are several differences: the instance and solver composition differ, they used a SAT-specific MPNN layer, whereas we employ a general-purpose GIN, and our baselines use the latest SATzilla 2024 features, which have shown significantly better results than the previous version [Shavit and Hoos, 2024]. Since the authors did not publish their code, we were unable to include their method as a baseline in our study. Among the three baselines based on hand-crafted features, we observe that multi-class classification underperforms both pairwise classification and regression, leaving a negative gap on the small and medium-sized datasets. This highlights that algorithm selection is not a simple multi-class classification problem. In that formulation, the model loses valuable information about the performance of algorithms other than the best one. Finally, we find more gaps closed for the large dataset across all three baselines, as it includes harder instances. As times increase, the benefit of algorithm selection grows, since feature computation accounts for a smaller fraction of total computation time. Moreover, for harder instances, multiple solvers frequently time out, so choosing a solver that successfully solves the instance becomes especially valuable, given the additional penalty imposed by the PAR score.

3.3.2. Combinatorial optimization: Learning to predict optimal solution objectives

Combinatorial optimization (CO) lies at the intersection of optimization, operations research, discrete mathematics, and computer science [Korte and Vygen, 2012]. The goal is to find a solution from a discrete set that optimizes a given objective under constraints. Formally, a *combinatorial optimization problem instance* I is described by a tuple (\mathcal{Q}, F, w) :

- $\mathcal{Q}(I)$ is a *finite set*,
- $F(I) \subseteq 2^{\mathcal{Q}(I)}$ is the set of *feasible solutions*, and
- $w: \mathcal{Q}(I) \rightarrow \mathbb{R}$ assigns *weights* to elements of $\mathcal{Q}(I)$.

Table 10: **SAT Solving.** Algorithm selection results (gap closed; higher is better).

Instances	Method	VG	VCG	LCG
SMALL	GIN	0.05 \pm 0.00	0.00 \pm 0.00	-0.02 \pm 0.02
	PC	–	0.03 \pm 0.02	–
	PR	–	0.48 \pm 0.03	–
	MC	–	-0.32 \pm 0.02	–
MEDIUM	GIN	–	–	–
	PC	–	0.13 \pm 0.02	–
	PR	–	0.44 \pm 0.02	–
	MC	–	-0.13 \pm 0.02	–
LARGE	GIN	–	–	–
	PC	–	0.33 \pm 0.01	–
	PR	–	0.54 \pm 0.02	–
	MC	–	0.23 \pm 0.02	–

The *cost* or *objective value* of a solution $S \in F(I)$ is given by $c(S) = \sum_{\omega \in S} w(\omega)$. The goal is to find an optimal solution $S_I^* \in F(I)$ minimizing c over the feasible set.⁶

CO plays a central role in many practical applications, including vehicle routing, scheduling, and resource allocation [Paschos, 2014], underscoring the importance of solving such optimization problems effectively. Graphs play a central role in CO due to the inherently discrete structure of many problems and the prevalence of network data. Problems such as max-cut and the independent set problem are naturally expressed on graphs. Among the 21 NP-complete problems identified by Karp [1972], ten are graph problems; others, such as set covering, can also be formulated in graph terms. Specifically, variable-constraint relationships often induce bipartite graphs, where variables are connected to the constraints in which they appear. These structural patterns provide strong inductive biases for graph learning.

Although CO problems are often computationally hard due to their discrete and non-convex nature [Karp, 1972], they can usually be solved effectively in practice using exact [Korte and Vygen, 2012], heuristic [Boussaïd et al., 2013], or approximation [Vazirani, 2010] methods. Classical research has focused on individual problem instances. However, in many real-world applications, structurally similar problems occur repeatedly. This motivates learning-based or data-driven approaches [Bengio et al., 2021, Cappart et al., 2021, Gasse et al., 2022], which aim to generalize across families of related instances.

CO problems are particularly well-suited for learning-based research, i.e., their hardness [Karp, 1972] motivates the use of MPNNs or GNNs as efficient surrogates for solving large instances. Since many are naturally graph-structured, solving them effectively requires expressive architectures [Chen et al., 2023, 2024]. Additionally, large synthetic datasets can be generated for robust benchmarking. Traditional methods can yield optimal solutions for small cases and strong approximations for larger ones, supporting both supervised training and generalization studies. The objective value provides a clear quantitative signal, making CO an ideal testbed for advancing graph learning.

⁶Without loss of generality, we assume minimization.

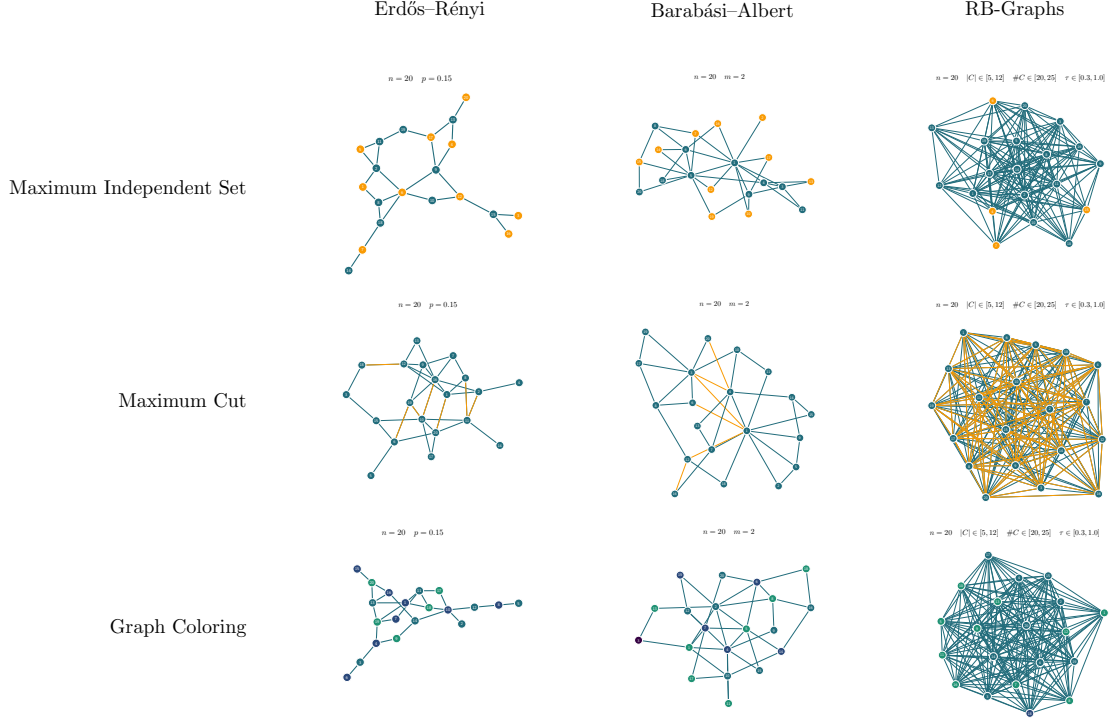


Figure 6: Down-scaled sample graphs and solutions across all graph generators and all performed tasks for the *Combinatorial Optimization* datasets with our chosen parameters.

Related work Many recent learning-based optimization work rely on synthetic data [Toenshoff et al., 2021, Tönshoff et al., 2023, Zhang et al., 2023, Karalias and Loukas, 2020], either RB graphs [Xu et al., 2007], Erdős–Rényi (ER) graphs [Erdős and Rényi, 1960], or Barabási–Albert (BA) graphs [Albert and Barabási, 2002]. Some also utilize pre-existing datasets from earlier graph benchmarks, e.g., [Karalias and Loukas, 2020] uses TUDatasets [Morris et al., 2020], and Li et al. [2022] uses Planetoid datasets [Yang et al., 2016]. Earlier efforts have also produced benchmarks for specific graph CO problems. For graph coloring, examples include hard 3-colorability datasets featuring cliques [Mizuno and Nishihara, 2007, 2008], queen graphs [Chvátal, 2004], Latin square graphs [Gomes and Shmoys, 2002], K -Insertions graphs [Caramia and Dell’Olmo, 2002a], and K -FullIns graphs [Caramia and Dell’Olmo, 2002b]. The DIMACS benchmark collection [Rossi and Ahmed, 2015] provides hundreds of real-world networks and problem instances across various CO domains. Still, their heterogeneity and limited number of instances per category make them less suited for modern machine learning pipelines. More recently, Nath and Kuhnle [2024] introduced a max-cut benchmark covering a variety of graph classes. Our motivation differs from these prior works. We aim to design a unified set of graph datasets shared across multiple CO tasks, enabling direct comparison between methods in a consistent experimental setting. While some prior work generates random instances for individual problems, we standardize the process by fixing both the generation procedures and the training-validation splits, ensuring that all methods compare on the same instances. Figure 6 provides an overview of our graph generators, the tasks we perform, and the parameters we chose for generation.

Description of the learning tasks We include tasks for both supervised and unsupervised learning settings. For the supervised setting, the objective is to train a graph learning model to predict the optimal objective value of given CO instances. Given a set of CO problem instances \mathcal{I} with corresponding optimal solutions S_I^* , and a model $m: \mathcal{I} \rightarrow \mathbb{R}$, the learning task is to minimize the mean absolute error between the predicted and true objective values,

$$\frac{1}{|\mathcal{I}|} \sum_{I \in \mathcal{I}} |m(I) - c(S_I^*)|.$$

While this setup focuses on predicting the objective value rather than producing explicit solutions, it offers a practical advantage: it avoids the challenge of defining a meaningful loss function when multiple distinct optimal solutions exist. This simplification enables consistent, well-defined evaluation and learning.

The supervised setting relies on solver-generated solutions, which can be computationally infeasible for large instances. This motivates the unsupervised setting, which is valuable when ground-truth solutions are not available or expensive to obtain, and directly targets solving the CO problem. We provide a differentiable surrogate loss function $\mathcal{L}: \mathbb{R}^{|\mathcal{Q}(I)|} \rightarrow \mathbb{R}$ as well as decoders $d: \mathbb{R}^{|\mathcal{Q}(I)|} \rightarrow F(I)$ for each CO problem. The model $m: \mathcal{I} \rightarrow \mathbb{R}^{|\mathcal{Q}(I)|}$ is trained in an unsupervised fashion to predict a score for each variable that indicates whether it belongs to the solution set, minimizing

$$\frac{1}{|\mathcal{I}|} \sum_{I \in \mathcal{I}} \mathcal{L}(m(I)).$$

At test time, the model’s output scores are converted into a feasible solution to the CO problem using the decoder. The model’s performance is measured based on the objective value of the decoded solution, $c(d(m(I)))$. This setup is widely used in graph learning for CO literature [Karalias and Loukas, 2020, Min et al., 2022, Wenkel et al., 2024]. We adapt our surrogate loss functions and decoders from this existing literature.

Details on the datasets We consider three representative hard combinatorial optimization problems on graphs, the *maximum independent set* (MIS), the *max-cut*, and the *graph coloring problem*. These problems span a broad spectrum of structural properties and computational challenges.

Given a problem defined on a graph $G = (V(G), E(G))$, the MIS problem is to find the largest subset of non-adjacent nodes, formally,

- $\mathcal{Q}(I) := V(G)$
- $F(I) := \{S \subseteq V(G) \mid \forall u, v \in S, (u, v) \notin E(G)\}$
- $w: V(G) \rightarrow \mathbb{R}$, in the unweighted case $w(v) := -1$.

The objective is to find $S_I^* \in F(I)$ minimizing $c(S) := \sum_{v \in S} w(v)$.

The max-cut problem seeks a 2-way partition of the node set such that the total weight of edges across the cut is maximized, i.e.,

- $\mathcal{Q}(I) := E(G)$,
- $F(I) := \{S \subseteq E(G) \mid \exists V'(G) \subset V(G), \forall (u, v) \in S: u \in V(G), v \in V(G) \setminus V'(G)\}$,
- $w: E(G) \rightarrow \mathbb{R}$, in the unweighted case $w(e) := -1$.

Table 11: Parameters for CO problems generation.

Generator	Size	Nodes	Nodes/Clique	Cliques	Tightness	Edge Prob.	Attached Edges
RB	small	[200, 300]	[5, 12]	[20, 25]	[0.3, 1]	-	-
	large	[800, 1200]	[20, 25]	[40, 55]	[0.3, 1]	-	-
ER	small	[200, 300]	-	-	-	0.15	-
	large	[700, 800]	-	-	-	0.15	-
BA	small	[200, 300]	-	-	-	-	2
	large	[700, 800]	-	-	-	-	2

The objective is to find $S_I^* \in F(I)$ minimizing $c(S) := \sum_{e \in S} w(e)$.

Graph coloring is the problem of assigning at most k colors to the nodes such that adjacent nodes receive different colors. Inspired by the assignment-based model [Jabrayilov and Mutzel, 2018], it can be formulated in search of a coloring function $f: V(G) \rightarrow [k]$, such that

- $\mathcal{Q}(I) := [k]$,
- $F(I) := \{S \subseteq [k] \mid \forall (u, v) \in E(G): f(v) \neq f(u) \wedge \forall v \in V(G): f(v) \in S\}$,
- $w: \mathcal{Q}(I) \rightarrow \{1\}$.

The objective is to find the best $S_I^* \in F(I)$, such that the minimum number of colors is used, $c(S) := \sum_{s \in S} w(s)$.

To construct the datasets, we first define how the input graphs are generated. We consider three well-established random graph models: RB graphs, ER graphs, and BA graphs. These models are widely used in machine learning to solve CO problems. The diversity and difficulty of each dataset are controlled via graph generation parameters. Specifically,

- for RB graphs, we specify integers n (number of cliques), k (nodes per clique), and a float p (constraint tightness). The total number of nodes is kn , and we discard graphs whose size falls outside a predefined range.
- For BA graphs, we control the number of nodes and the parameter m , which determines how many edges are attached from each new node.
- For ER graphs, we use the number of nodes and the edge probability p , which controls the probability that an edge exists between any given pair of nodes.

We generate 50 000 instances for each dataset and provide both small-scale and large-scale variants. Table 11 shows a summary of the parameters used for graph generation. For RB graphs, parameters are taken from Zhang et al. [2023], Sanokowski et al. [2024], Wenkel et al. [2024], Sun et al. [2022]. Parameters for large ER graphs are from Böther et al. [2022], Qiu et al. [2022], Sun and Yang [2023], Yu et al. [2024]. Parameters for large BA graphs are from Böther et al. [2022]. The parameters for ER-small and BA-small are adjusted to match the graph size of RB-small. When a parameter is specified as a range, it is sampled uniformly at random for each instance. The only exception to this is the number of nodes in RB graphs, which is determined as described above.

We provide datasets in both PyTorch Geometric format [Fey and Lenssen, 2019, Fey et al., 2025] and NetworkX format [Hagberg and Conway, 2020]. Each instance retains only its adjacency matrix, and no node features are included.

For all the instances from various datasets, we use KaMIS [Lamm et al., 2016] for heuristic MIS solutions. The solution to max-cut is obtained by formulating it as an integer programming problem and solving it with Gurobi Optimization, LLC [2024], with a timeout of 3600 seconds. We use GCol [Lewis and Palmer, 2025] for a heuristic graph chromatic number, with a maximum of 10^8 search iterations. The labeled datasets in our benchmark support both supervised learning, e.g., formulating a regression task to predict objective values, and unsupervised learning, where the goal is to find high-quality feasible solutions without access to ground-truth labels. The generality of the (\mathcal{Q}, F, w) framework makes it applicable to a wide range of CO problems, including all those proposed in our benchmark.

Experimental evaluation and baselines For the supervised setting, we benchmark our baselines on the MIS problem. The task is to predict the CO objective value for the MIS problem. We train all models using the MAE as the loss function and report the final test MAE for evaluation. For the unsupervised setting, we evaluate on all three CO problems, i.e., MIS, max-cut, and graph coloring. The models are trained unsupervised using a problem-specific surrogate loss function. At test time, the model’s output scores are converted into a feasible solution to the CO problem using a decoder. The CO problem’s objective function is then used as a metric to measure the quality of the solutions obtained this way. We conduct experiments on small and large synthetic graphs from the RB, ER, and BA families. We compare four baseline models: GIN, GT, MLP, and DeepSets, using the hyperparameters listed in Table 26. Our proposed model uses the encoder-decoder architecture. The encoder, an MLP, processes node features derived from RWSE [Dwivedi et al., 2022b] and node degrees. The processor module is the only part that differs between baselines and performs the bulk of the calculations. It is followed by a decoder that generates node representations. For the supervised setting, we apply summation aggregation to obtain a scalar graph-level prediction as the final output. For the unsupervised setting, we leave the node-level scores as the output.

Results The complete results for the supervised learning task are presented in Table 12. Among the baselines, GIN achieves the best performance across most datasets. We attribute this to MPNNs’ strong inductive bias, which aligns well with the structure of graph-based CO problems. DeepSet generally outperforms the MLP baseline, except for the ER graphs. This suggests that global information aggregation is beneficial for this task. Conversely, the GT performs poorly on some datasets. We hypothesize that this is due to the training difficulties associated with this task. Table 13 shows the baseline results for unsupervised CO. We report the average objective value of solutions obtained by running the decoder on the model’s output scores for test-set problem instances. Out of the four baselines, GIN performs best across all three CO problems, with some exceptions. As expected, the graph-based models GIN and GT generally perform better than MLP and DeepSet. One exception is graph coloring on the (very sparse) BA graphs, where DeepSet outperforms the other two models on both graph sizes. Note that our baselines do not utilize diffusion or other advanced architectures or techniques tailored explicitly for CO. Their performance is therefore much weaker compared to methods that do use them, e.g. Sanokowski et al. [2024], Zhang et al. [2023]. Also note that most learning-based methods currently cannot compete with exact solvers and some hand-crafted heuristics in terms of solution quality, but are often much quicker [Sun and Yang, 2023, Sanokowski et al., 2024, Zhang et al., 2023].

Table 12: **Combinatorial Optimization.** Results for each CO dataset with supervised learning (MIS).

Dataset	Method	Size	
		Small	Large
RB graph	GIN	0.491 \pm 0.099	2.125 \pm 0.484
	GT	4.112 \pm 2.353	0.915 \pm 0.235
	MLP	1.583 \pm 0.052	1.437 \pm 0.520
	DeepSet	0.918 \pm 0.186	1.427 \pm 0.224
ER graph	GIN	0.234 \pm 0.191	0.352 \pm 0.265
	GT	6.486 \pm 8.101	9.641 \pm 15.335
	MLP	0.751 \pm 0.767	0.914 \pm 0.307
	DeepSet	0.756 \pm 0.711	2.244 \pm 0.364
BA graph	GIN	0.292 \pm 0.041	0.111 \pm 0.016
	GT	3.481 \pm 3.446	1.829 \pm 1.383
	MLP	2.825 \pm 0.949	3.383 \pm 0.504
	DeepSet	2.304 \pm 0.262	3.362 \pm 1.491

3.3.3. Algorithmic reasoning: Learning to simulate algorithms

In addition to SAT, many real-world tasks depend on the efficient solution of graph algorithms. Given the active exploration of the intersection of algorithms and neural networks across domains [Estermann et al., 2024, Fan et al., 2024a, Kaiser and Sutskever, 2016, Zaremba and Sutskever, 2014], our goal is to provide dedicated datasets for graph algorithmic reasoning. Prior work [Velickovic et al., 2020b, Xu et al., 2020, Bounsi et al., 2024] and benchmarks such as CLRS [Velickovic et al., 2022] have demonstrated that GNN architectures can achieve strong performance on graph problems when provided with hints and graph invariants—tasks that require substantial theoretical expressiveness from graph learning models [Arvind et al., 2020]. To broaden this research area, we contribute large-scale datasets for several common graph algorithm tasks, expanding the landscape of neural algorithmic reasoning benchmarks. Figure 7 provides an overview of our graph generators, the tasks we perform and the parameters we chose for generation.

Related work Algorithmic reasoning has been adopted for various architectures [Li et al., 2024a, Velickovic et al., 2020a]. Apart from neural networks [Diao and Loynd, 2023, Mahdavi et al., 2023, Bounsi et al., 2024, Rodionov and Prokhorenkova, 2023] and reinforcement learning approaches [Estermann et al., 2024], Velickovic et al. [2022] propose the CLRS benchmark for a variety of algorithmic tasks, derived from the *Introduction to Algorithms* textbook [Cormen et al., 2009]. This benchmark comprises 30 algorithmic problems, each accompanied by hints to guide the solution. However, this benchmark does not include regression tasks and restricts learning tasks to specific algorithms. Furthermore, follow-up works investigated the importance of hints given in CLRS [Rodionov and Prokhorenkova, 2023] and proposed a variety of architectures for solving algorithmic tasks [Bevilacqua et al., 2023, Ibarz et al., 2022, Li et al., 2024a].

Table 13: **Combinatorial Optimization.** Results for each CO dataset with unsupervised learning.

Problem	Dataset	Method	Size	
			Small	Large
MIS (MIS size \uparrow)	RB	GIN	17.294 \pm 0.328	13.999 \pm 0.321
		GT	16.542 \pm 0.477	13.406 \pm 0.140
		MLP	16.105 \pm 0.097	13.040 \pm 0.214
		DeepSet	16.021 \pm 0.032	13.183 \pm 0.035
		Solver	20.803 \pm 1.817	42.547 \pm 4.449
MIS (MIS size \uparrow)	ER	GIN	25.418 \pm 0.407	26.276 \pm 0.408
		GT	22.984 \pm 0.473	24.980 \pm 0.292
		MLP	23.183 \pm 0.016	24.259 \pm 0.449
		DeepSet	23.050 \pm 0.061	24.220 \pm 0.056
		Solver	33.604 \pm 1.428	45.637 \pm 0.631
BA	BA	GIN	100.16 \pm 3.674	135.00 \pm 0.720
		GT	99.579 \pm 6.448	114.26 \pm 0.601
		MLP	95.108 \pm 2.042	114.49 \pm 0.758
		DeepSet	95.076 \pm 0.173	114.89 \pm 0.016
		Solver	142.86 \pm 16.54	433.77 \pm 19.17
Maximum Cut (maximum cut size \uparrow)	RB	GIN	2106.7 \pm 14.62	24748. \pm 87.76
		GT	1925.7 \pm 32.75	21524. \pm 184.0
		MLP	1727.7 \pm 165.1	20357. \pm 249.6
		DeepSet	140.02 \pm 155.5	3575.9 \pm 730.0
		Solver	2920.1 \pm 97.23	33914. \pm 7861.
Maximum Cut (maximum cut size \uparrow)	ER	GIN	2327.9 \pm 24.78	20878. \pm 107.9
		GT	2172.7 \pm 91.75	16534. \pm 278.0
		MLP	1866.7 \pm 67.64	7335.4 \pm 57.49
		DeepSet	33.634 \pm 20.84	27.663 \pm 6.763
		Solver	2835.5 \pm 607.6	23884. \pm 1809.
Graph Coloring (number of colors used \downarrow)	BA	GIN	397.00 \pm 0.605	1044.1 \pm 0.649
		GT	363.76 \pm 0.639	986.93 \pm 3.128
		MLP	308.73 \pm 0.224	929.20 \pm 4.060
		DeepSet	1.0669 \pm 0.800	154.31 \pm 151.5
		Solver	460.91 \pm 50.13	1260.4 \pm 48.81
Graph Coloring (number of colors used \downarrow)	RB	GIN	25.166 \pm 0.288	55.513 \pm 0.526
		GT	25.146 \pm 0.253	55.562 \pm 0.648
		MLP	24.733 \pm 0.667	55.558 \pm 0.557
		DeepSet	26.723 \pm 0.189	71.051 \pm 0.604
		Solver	19.970 \pm 3.465	41.480 \pm 6.634
Graph Coloring (number of colors used \downarrow)	ER	GIN	16.182 \pm 0.202	34.587 \pm 0.545
		GT	16.188 \pm 0.201	34.385 \pm 0.413
		MLP	17.110 \pm 0.144	34.658 \pm 0.394
		DeepSet	18.266 \pm 0.018	55.345 \pm 0.551
		Solver	10.235 \pm 0.836	22.933 \pm 0.772
Graph Coloring (number of colors used \downarrow)	BA	GIN	5.1318 \pm 0.114	6.2028 \pm 0.283
		GT	5.0939 \pm 0.070	6.1167 \pm 0.086
		MLP	5.9900 \pm 0.127	9.4215 \pm 0.186
		DeepSet	3.2780 \pm 0.122	3.1981 \pm 0.239
		Solver	3.0000 \pm 0.000	3.0000 \pm 0.000

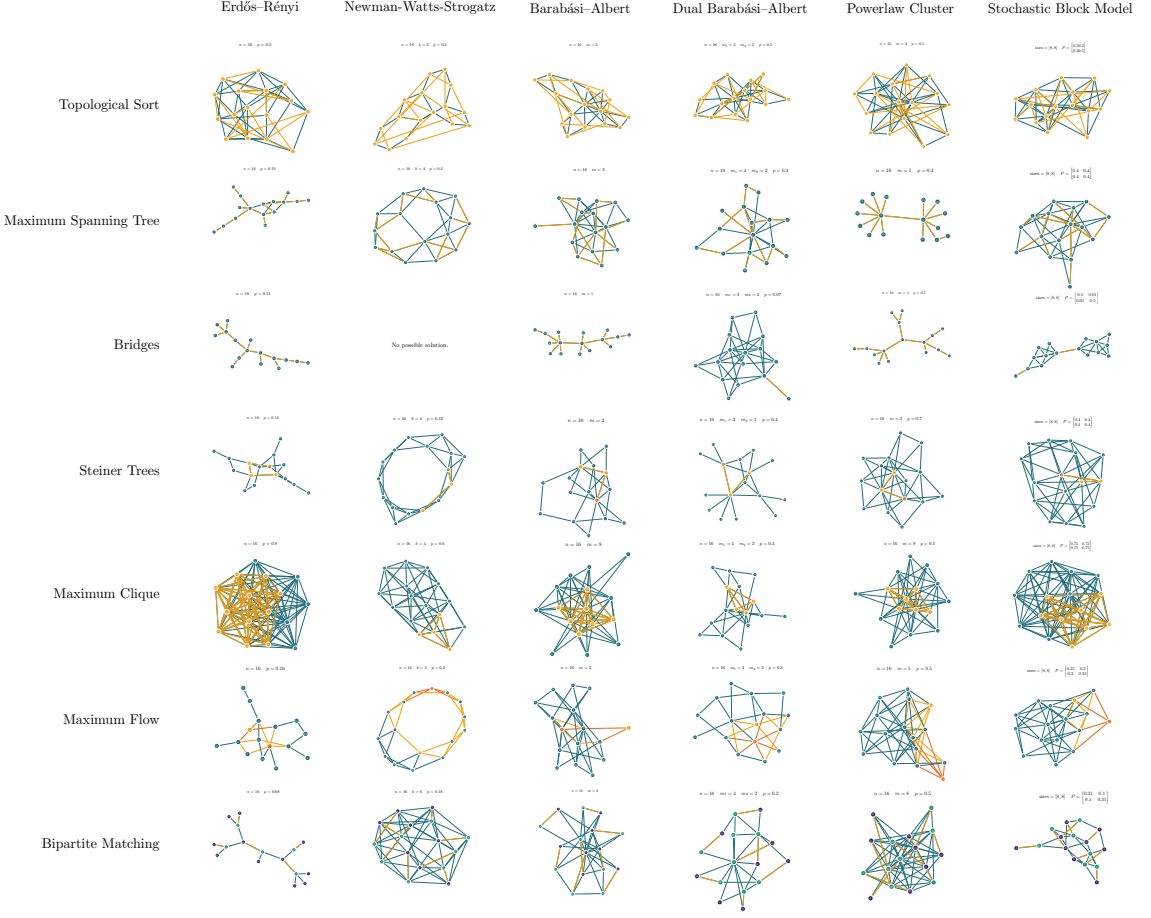


Figure 7: Example graphs and solutions across all graph generators and all performed tasks for the *Algorithmic Reasoning* datasets with our chosen parameters.

Description of learning task We consider a collection of seven algorithmic reasoning tasks, selected from classical graph problems studied in algorithmics. These tasks include computing the topological sorting [Kahn, 1962], identifying bridges in a graph, computing the minimum spanning tree [Kruskal, 1956], determining the maximum flow [Goldberg and Tarjan, 1986], finding the maximum clique, computing Steiner trees [Kou et al., 1981], and solving bipartite matching [Hopcroft and Karp, 1973]. Our task set spans different output granularities: node-level tasks (topological sorting, bipartite matching, max clique), edge-level tasks (bridges, minimum spanning tree, Steiner tree), and a graph-level task (max flow). To introduce additional modeling challenges, we provide three levels of difficulty per task, representing variations in the underlying graph distributions. Each task is formulated as either a binary classification or a regression problem. Given a set of graphs \mathcal{G}_A , an algorithmic reasoning task A , its ground-truth solution function S_A , and a model m , the goal is to train

$$m: \mathcal{G}_A \rightarrow \mathbb{R} \quad \text{or} \quad m: \mathcal{G}_A \rightarrow [0, 1],$$

depending on the task. The objective is to minimize the MAE between the model’s predictions and the ground-truth solution,

$$\frac{1}{|\mathcal{G}_A|} \sum_{G \in \mathcal{G}_A} |m(G) - S_A(G)|.$$

For binary classification tasks, we instead report the F1 score computed from the objective to maximize the accuracy between predictions and ground truth,

$$\frac{1}{|\mathcal{G}_A|} \sum_{G \in \mathcal{G}_A} \mathbb{1}(m(G) = S_A(G))$$

where $\mathbb{1}$ denotes the indicator function.

Details on the datasets For all algorithmic reasoning tasks, we work with sets of synthetically generated graphs. We begin by sampling graphs using a variety of graph generators, including Erdős–Rényi (ER) graphs [Erdős and Rényi, 1960], stochastic block model (SBM) graphs [Holland et al., 1983], power-law cluster (PC) graphs [Holme and Kim, 2002], Newman–Watts–Strogatz (NWS) graphs [Newman and Watts, 1999], Barabási–Albert (BA) graphs [Barabási and Albert, 1999], and dual Barabási–Albert (DBA) graphs [Moshiri, 2018]. During the sampling process, we ensure that each resulting graph is unique; otherwise, it is resampled. For each task, we choose generator parameters shown in Table 14 to yield meaningful distributions of task-specific properties. We further introduce the parameter of component connections, determining the number of random edges between disconnected components in a graph. This allows us to sample graphs with low edge probabilities without disconnected components. Additionally, based on the difficulty level, we adjust the probability distribution over the selected graph generators to further control the complexity of generated instances, as seen in Table 15. For minimum spanning tree computations, we also adjust the graph generator parameters, as indicated in Table 14, to require stronger generalization capabilities, as the same parameters proved too easy to generalize from. Ground-truth labels are computed using the NETWORKX library [Hagberg and Conway, 2020], which provides reference implementations of most of the required graph algorithms. For edge-level tasks, we also generate an edge-level representation

Table 14: Graph generation parameters for algorithmic reasoning tasks. The cc parameter denotes the number of connections between disconnected components in Erdős–Rényi graphs.

Generator	Param.	Top. Sort	MST	MST (shift)	Bridges	Steiner Trees	Max. Clique	Flow	Max. Matching
ER	p	0.3	0.19	0.17	0.11	0.14	0.9	0.16	0.08
	cc	1	1	1	1	1	1	1	1
NWS	k	2	4	2	-	4	4	4	6
	p	0.2	0.2	0.15	-	0.12	0.6	0.2	0.18
BA	m	2	3	2	1	2	8	3	3
	m_1	3	4	2	3	3	4	4	4
	m_2	2	2	1	1	1	2	2	2
DBA	p	0.5	0.3	0.05	0.07	0.4	0.3	0.3	0.2
	p	0.1	0.4	0.35	0.5	0.7	0.5	0.5	0.5
	m	3	1	5	1	3	9	5	8
SBM	p. mat.	$\begin{bmatrix} 0.5 & 0.2 \\ 0.2 & 0.5 \end{bmatrix}$	$\begin{bmatrix} 0.4 & 0.4 \\ 0.4 & 0.4 \end{bmatrix}$	$\begin{bmatrix} 0.31 & 0.01 \\ 0.01 & 0.31 \end{bmatrix}$	$\begin{bmatrix} 0.5 & 0.01 \\ 0.01 & 0.5 \end{bmatrix}$	$\begin{bmatrix} 0.4 & 0.4 \\ 0.4 & 0.4 \end{bmatrix}$	$\begin{bmatrix} 0.75 & 0.75 \\ 0.75 & 0.75 \end{bmatrix}$	$\begin{bmatrix} 0.35 & 0.3 \\ 0.3 & 0.35 \end{bmatrix}$	$\begin{bmatrix} 0.31 & 0.1 \\ 0.1 & 0.31 \end{bmatrix}$
	sizes	$1/2, 1/2$	$1/2, 1/2$	$1/2, 1/2$	$1/2, 1/2$	$1/2, 1/2$	$1/2, 1/2$	$1/2, 1/2$	$1/2, 1/2$

Table 15: Graph generation parameters for algorithmic reasoning tasks.

Split	Difficulty	ER	PC	NWS	BA	DBA	SBM
Train	EASY	1/3	0	1/3	0	1/3	0
	MEDIUM	1	0	0	0	0	0
	HARD	1	0	0	0	0	0
Valid/Test	EASY	1/6	1/6	1/6	1/6	1/6	1/6
	MEDIUM	1/6	1/6	1/6	1/6	1/6	1/6
	HARD	0	1/5	1/5	1/5	1/5	1/5

to support models that require tokenized input. Each task includes one million generated training graphs and 10 000 validation and test graphs. To assess generalization beyond function approximation, we fix the number of nodes in training graphs to 16, while setting validation and test graphs to have 128 nodes.

To further study generalization, we introduce size-generalization tasks, in which pre-trained models are evaluated on graphs with sizes ranging from 128 to 512 nodes. We exclude max-flow computation from size generalization, as the MAE scales with the number of nodes in the flow network and is therefore not indicative of size generalization. This setup enables an empirical analysis of how well models extrapolate to unseen graph sizes. Except for the topological sorting, Steiner tree, and bipartite matching tasks, no node features are given. For the minimum spanning tree, max flow, and Steiner tree tasks, corresponding edge weights are included as edge attributes.

Experimental evaluation and baselines We use the encoder-processor-decoder pipeline described in Section B. For node and graph-level tasks, the pipeline is applied directly with the task-specific encoder described below. Since the graph transformer baseline expects node-level tokenization, we provide an additional graph transform. We leverage the following edge transform which allows us to provide node level tokenization on a modified graph G' obtained from the original graph G , with $V(G') := \{(v, v) \mid v \in V(G)\} \cup E(G)$ and $E(G') := \{((u, v), (w, z)) \mid u = w \vee u = z \vee v = w \vee v = z\}$.

Since most of our tasks provide only node or edge features, we use learned vectors, as described in the encoder, for the remaining embeddings. Across all datasets, we employ one-layer linear embeddings for both integer and real-valued features. Depending on the node, edge, or graph level tasks, the decoder applies linear layers that represent the classification or regression target. In the case of bridges, minimum spanning tree, Steiner trees, max clique and bipartite matching a binary classification target is used for node or edge level predictions. For flow and topological sorting, a one-dimensional regression target is used instead. For pretrained models used in size generalization experiments, we use the model directly as encoder, processor, and decoder. However, the input graph size is increased. In contrast to complete training examples, we conduct a few-shot scenario with only 1 000 graphs to allow for fast inference. In addition, we do not consider the flow task here because it is a regression setting. Throughout all experiments, we use the same random seed for a pretrained model to enable comparison to the 128-node test set.

Results We report results on all datasets for each of the three selected difficulties. These are denoted using the terms EASY, MEDIUM, and HARD to reflect the additional generalization requirements introduced by out-of-distribution sampling. For classification tasks, we report F1 scores, and for

regression tasks, we report MAE. All results are grouped by their respective estimated task difficulty in Table 16 and Table 17 below. Additionally, we report size generalization results using pre-trained baselines from the MEDIUM setting of our training procedure. For this, we evaluate each pre-trained model across 128 to 512 graph nodes. Results are provided in Table 18. For minimum spanning tree, max clique and max matching datasets show improved performance with the graph transformer baseline. However, on the max flow, bridges, and Steiner tree datasets, the GIN baseline model performs better across the proposed difficulty levels. Furthermore, we observe a reduction in F1 scores with increasing difficulty across datasets, highlighting the varying generator selections in the training data. However, the differences are not as pronounced as expected for the bridges dataset. We further observe that the GIN baseline is inconsistent across seeds for the minimum spanning tree and Steiner tree tasks, whereas the graph transformer baseline does not exhibit similar issues. Overall, the performance of both baselines is the lowest for Steiner trees and max clique tasks, indicating that these tasks are more complex for graph learning baselines to learn. Similar to the results obtained in the CLRS benchmark [Velickovic et al., 2022] and by Müller et al. [2024b] for an expressive graph transformer architecture, MST, bridges, and topological sorting provide more manageable tasks for graph learning baselines. We note that, despite previous benchmarks such as CLRS, there are currently no other baseline results on the synthetic algorithmic reasoning datasets we provide.

In the case of size generalization, we observe that both baselines are relatively robust to test graph size scaling. However, we observe that the generalization capability to graph size is task-dependent, with minimum spanning tree, and Steiner tree tasks improving with larger graphs. Nonetheless, we note that this behavior may be observed due to shifts in average degree and node connectivity, using the same parameters as in test set generation, since every graph generator method selected scales with the number of nodes. Nonetheless, performance is decreasing for topological sorting, max matching, and max clique tasks, highlighting the inability of our selected baselines to be size-generalization invariant across all tasks.

3.4. Earth systems

The earth systems domain in **GRAPHBENCH** includes graph learning tasks built from geospatial, environmental, and climate data. Nodes represent locations, sensors, or regions, and edges capture spatial or physical relationships. These tasks are key for applications such as weather forecasting, climate impact assessment, and resource management. They test whether graph-based models can integrate heterogeneous features, capture long-range dependencies, and generalize across time and space for robust environmental decision-making.

3.4.1. Weather forecasting: Medium-range atmospheric state prediction

Weather forecasting has long been critical for agriculture, energy, and public safety [Diehl et al., 2013, Ramar and Mirnalinee, 2014]. Traditional *numerical weather prediction* (NWP) is accurate but relies on computationally expensive physics-based simulations [Bauer et al., 2015]. Recent machine learning methods offer faster, scalable alternatives that can outperform NWP for medium-range forecasts and extreme events—while improving uncertainty quantification [Price et al., 2023]. Earth system data are sparse, irregular, and interconnected [Reichstein et al., 2019], with interactions spanning scales from local convection to planetary waves [Bauer et al., 2015]. Graph-based models naturally capture these multi-scale, non-Euclidean dependencies, enabling flexible representations of local and global atmospheric interactions. Figure 8 provides an intuitive image of how the graph

Table 16: Resulting F1 scores for algorithmic reasoning datasets, including minimum spanning tree, bridge finding, Steiner tree computation, max clique, and max matching.

Task	Difficulty	Model	F1
MST	EASY	GIN	0.6906 \pm 0.1655
		GT	0.8566 \pm 0.0068
	MEDIUM	GIN	0.7288 \pm 0.0894
		GT	0.8504 \pm 0.0148
	HARD	GIN	0.6107 \pm 0.2015
		GT	0.8421 \pm 0.0115
Bridges	EASY	GIN	0.9831 \pm 0.0184
		GT	0.9269 \pm 0.0103
	MEDIUM	GIN	0.9622 \pm 0.0077
		GT	0.8762 \pm 0.0258
	HARD	GIN	0.968 \pm 0.0178
		GT	0.8897 \pm 0.0304
Steiner Trees	EASY	GIN	0.6691 \pm 0.0288
		GT	0.6691 \pm 0.0112
	MEDIUM	GIN	0.5628 \pm 0.1100
		GT	0.5672 \pm 0.0790
	HARD	GIN	0.5516 \pm 0.2368
		GT	0.5212 \pm 0.0219
Max Clique	EASY	GIN	0.4584 \pm 0.0101
		GT	0.5407 \pm 0.0088
	MEDIUM	GIN	0.3996 \pm 0.0852
		GT	0.4859 \pm 0.0017
	HARD	GIN	0.4102 \pm 0.0820
		GT	0.4868 \pm 0.0013
Max Matching	EASY	GIN	0.7527 \pm 0.0051
		GT	0.7402 \pm 0.0172
	MEDIUM	GIN	0.6399 \pm 0.0231
		GT	0.6915 \pm 0.009
	HARD	GIN	0.6595 \pm 0.0164
		GT	0.6743 \pm 0.0038

Table 17: Resulting MAE for topological sorting and flow.

Task	Difficulty	Model	MAE
Topological Sorting	EASY	GIN	0.1001 ± 0.0089
		GT	0.116 ± 0.0058
	MEDIUM	GIN	0.1537 ± 0.0031
		GT	0.1305 ± 0.0094
	HARD	GIN	0.1301 ± 0.0046
		GT	0.1532 ± 0.0214
Flow	EASY	GIN	3.4387 ± 0.0631
		GT	4.2737 ± 0.0646
	MEDIUM	GIN	9.5960 ± 0.1707
		GT	6.3786 ± 0.4262
	HARD	GIN	9.5061 ± 0.1265
		GT	6.4833 ± 0.0869

Table 18: Size generalization results on algorithmic reasoning datasets from Section 3.3.3. Each column represents an evaluation on 1000 graphs with the given number of nodes (128–512). For each experiment, the same generation parameters were used as in the results presented in Table 16 and Table 17. OOT denotes the case where the underlying size generalization data was not computed within 24 hours of computation on a single cluster node. All generated graphs are based on the *MEDIUM* difficulty setting. We use the same single seed for each pretrained model from each task to provide inference results on different sizes.

Dataset (Score)	Model	128	192	256	384	512
Topological Sorting (MAE)	GT	0.1346	0.1730	0.1827	0.2018	0.2071
	GIN	0.1492	0.181	0.1981	0.2015	0.2179
MST (F1)	GT	0.8720	0.8773	0.8891	0.8874	0.8817
	GIN	0.6103	0.8132	0.8605	0.8765	0.8823
Bridges (F1)	GT	0.8799	0.8842	0.8959	0.9049	0.9118
	GIN	0.9579	0.9213	0.9190	0.9203	0.9212
Steiner Trees (F1)	GT	0.5160	0.5322	0.5221	0.5762	0.5578
	GIN	0.5499	0.5739	0.6338	0.6651	0.6502
Max Clique (F1)	GT	0.4877	0.4849	0.4890	0.4915	0.4931
	GIN	0.3496	0.3112	0.3148	0.2926	0.2673
Max Matching (F1)	GT	0.7010	0.6552	0.6206	0.5770	OOT
	GIN	0.6271	0.6326	0.6372	0.6382	OOT

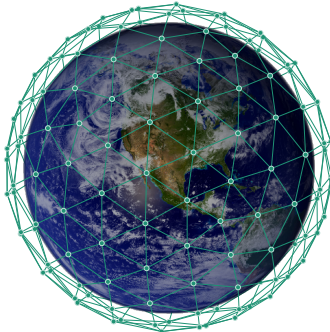


Figure 8: Down-scaled version of our node icosahedron spanning the globe. Each node contains weather variables of the corresponding location across 13 pressure levels.

icosahedron spans the globe.

Related work The idea of utilizing machine learning models for weather forecasting first emerged in 2020, when Rasp et al. [2020] and Weyn et al. [2020] employed CNN architectures to predict global weather at resolutions of 5.625° and 1.9° , respectively. A key breakthrough occurred when Keisler [2022] first applied MPNNs to more naturally represent the globe, enabling the prediction of 3D states 6 hours ahead and facilitating multi-day forecasts. This approach has already achieved a skill comparable to that of 1° global NWP (GFS/ECMWF) on specific metrics, outperforming prior data-driven models. Building on this idea, Lam et al. [2023] introduced *GraphCast*, a multi-scale MPNN-based system that delivers today’s forecasts at 0.25° resolution. *GraphCast* achieved unprecedented accuracy, outperforming even ECMWF’s *high-resolution deterministic model* (HRES) out to ten days. The success of these deterministic forecasts raised the question of probabilistic prediction. Price et al. [2023] introduced *GenCast*, a generative weather model that produces an ensemble of forecasts rather than a single deterministic run. For this, they used a diffusion-based approach built on an MPNN backbone, outperforming ECMWF’s *ensemble system* (ENS), the world’s top operational probabilistic forecast on over 97% of evaluated metrics. Several other advances can be noted. Oskarsson et al. [2024] have proposed Graph-EFM, a model featuring a hierarchical GNN that seamlessly handles global and regional forecasts. With *OneForecast*, Gao et al. [2025] have introduced an MPNN framework using nested multi-scale graphs and adaptive message passing to improve local extreme event predictions within a global context. These works indicate a trend toward hybrid solutions that densify graphs in target regions for high-resolution detail while maintaining global consistency. Current state-of-the-art models, such as Pangu-Weather [Bi et al., 2022], Aurora [Bodnar, 2024], and FGN [Alet et al., 2025], all present excellent results that, in many areas, far exceed those of conventional NWP methods. It is important to note, however, that while machine learning-based approaches exceed NWP skill on tested time scales, they do not explicitly enforce conservation laws. Over long integration horizons, this can lead to subtle physical drifts that may limit specific climate-related uses. This becomes particularly relevant under regime shifts, for example, caused by climate change, that lie outside the distributions the models were trained on. Furthermore, compared to NWP models, ML-based approaches offer very limited interpretability, functioning mainly as black boxes.

Description of the learning task The objective of the task is to model medium-range weather evolution by predicting the residual change in the atmospheric state over a fixed 12-hour time horizon. Specifically, given an initial snapshot of the current atmospheric state, the model forecasts the twelve-hour future change in meteorological variables. To achieve this, the initial normalized grid values, which contain atmospheric data from various pressure levels at each grid point, are mapped to learned node attributes on an icosahedral node mesh using a single MPNN layer, as described in GraphCast [Lam et al., 2023]. Several rounds of message passing are then performed on this icosahedron, and the resulting states are mapped back to the grid using a single MPNN layer. This process yields a residual change in the atmospheric variables, which is then added to the original data to obtain an updated weather state twelve hours after the initial timestep. The training objective is a spatially and variable-weighted *mean-squared error* for the twelve-hour-ahead prediction, inspired by the training object used in GraphCast [Lam et al., 2023]. For each verification time $d \in D$, the model ingests x_{d-2} and predicts a residual change Δx , yielding $\hat{x}^d = x_{d-2} + \Delta x$. The loss compares \hat{x}^d with x^d . The loss function thus corresponds to

$$\mathcal{L}(x^d, \hat{x}^d) = \frac{1}{|D| |G| \sum_{j \in J} |L_j|} \sum_{d \in D} \sum_{i \in G} \sum_{j \in J} \sum_{\ell \in L_j} a_i w_j s_{j,\ell} (\hat{x}_{i,j,\ell}^d - x_{i,j,\ell}^d)^2,$$

with level weights

$$s_{j,\ell} = \begin{cases} \frac{P_\ell}{\frac{1}{|L_j|} \sum_{m \in L_j} P_m}, & \text{if } j \text{ is multi-level, e.g. atmospheric variables,} \\ 1, & \text{if } j \text{ is single-level, e.g. surface variables,} \end{cases}$$

where D is the set of forecast date-times, G the grid cells, J the variables, L_j the pressure levels for variable j , $a_i = \frac{\cos(\text{lat}_i)}{\frac{1}{|G|} \sum_{k \in G} \cos(\text{lat}_k)}$ are mean-normalized latitude weights, w_j are variable weights, and P_ℓ are the pressure levels. Predicting a residual change Δx rather than an absolute value improves stability and generalization [He et al., 2020].

Details on the dataset We utilize reanalysis data from the ERA5 dataset, which has been preprocessed via the WeatherBench2 pipeline [Rasp et al., 2024]. Multiple resolutions of this dataset are available. We use a downsampled version containing a 64×32 equiangular grid, employing a conservative area-preserving interpolation. ERA5 data has a temporal resolution of six hours, with timesteps at 0h, 6h, 12h, and 18h. Each weather state contains 62 physical and derived variables: 15 are defined across the 13 pressure levels, and 47 are defined at the surface. Of those, we only use five variables for the surface and six for the atmospheric levels each, as done by Price et al. [2023]. The pressure-level variables include temperature, humidity, and wind speed. The surface-level variables also include more general information about the location, such as a land-sea mask, sea level pressure, and precipitation.

We provide a dataset with the aforementioned resolution of 64×32 from ERA5, processed by the WeatherBench2 pipeline. It includes the original grid data as a 3D graph, the icosahedron as a mesh graph, and the mapping of edges between the two. The weights of this mapping must be learned during training, but the mappings themselves are fixed and can therefore be provided as static information.

The 3D grid graph contains 2 048 nodes, each linked by a directed edge to one of the 2 562 mesh nodes of the icosahedron. Together, these two structures form a single graph with 4 610 nodes and

59 667 edges. Each grid node contains information about five surface variables and six atmospheric variables across 13 pressure levels ranging from 50hPa to 1 000hPa. For the exact variables, see Table 19.

Experimental evaluation and baselines For the evaluation, we report an unweighted mean-squared error for each variable j ,

$$\text{MSE}_j(x^d, \hat{x}^d) = \frac{1}{|D| |G| |L_j|} \sum_{d \in D} \sum_{i \in G} \sum_{\ell \in L_j} (\hat{x}_{i,j,\ell}^d - x_{i,j,\ell}^d)^2,$$

and an unweighted mean-squared error over all variables,

$$\text{MSE}_{\text{all}}(x^d, \hat{x}^d) = \frac{1}{|D| |G| \sum_{j \in J} |L_j|} \sum_{d \in D} \sum_{i \in G} \sum_{j \in J} \sum_{\ell \in L_j} (\hat{x}_{i,j,\ell}^d - x_{i,j,\ell}^d)^2.$$

It should be noted here that the success of a weather forecast can be measured in many ways other than just the mean-squared error. For example, *WeatherBench 2* [Rasp et al., 2024] provides a comprehensive overview of various metrics and their relevance.

In addition to a 12-hour forecast, it is possible to predict the weather autoregressively over more extended periods. For example, the 12-hour forecast can be used as input for another 12-hour forecast. GraphCast [Lam et al., 2023] employs a six-step process, i.e., a three-day forecast. GenCast [Price et al., 2023] can even generate weather forecasts for up to 15 days.

Results In Table 19 we present results for each weather variable at three pressure levels, aligning with the results obtained in WeatherBench2 [Rasp et al., 2024], enabling an easily accessible comparison of weather forecasting models with traditional weather forecasting baselines. For comparative models like GraphCast and Persistence, only selected results are available. Thus, we compare against those in particular. However, we also account for cumulative errors across all pressure levels in the underlying data. Throughout our evaluation, we provide a 12-hour forecast prediction across all variables. Our baselines establish a transparent and reproducible lower bound for medium-range weather forecasting. While they do not reach the performance of Persistence or specialized systems like GraphCast, this is expected given their simpler architecture, shorter training time, and deliberately straightforward setup. Several factors contribute to this outcome. Unlike specialized systems, our models were trained for substantially fewer iterations, with fewer computing resources and without extensive hyperparameter optimization. We deliberately prioritized transparency and reproducibility over complexity in the architectural design. Our training setup is intentionally simple and does not incorporate domain-specific refinements, such as positional edge features, which are known to improve forecast skill. Moreover, medium-range weather forecasting is a particularly demanding task that often benefits from specialized evaluation protocols, whereas our assessment relies on a basic, uniform metric. Importantly, the purpose of this baseline is not to achieve state-of-the-art performance. Its main contribution is to provide a transparent, reproducible lower bound that serves as a precise reference point against which future graph learning methods can be compared.

4. Format, licensing, and long-term access

All GRAPHBENCH datasets are distributed as PyG objects with graph data, and raw data is also available in HDF5 for long-term compatibility. Data is released under open licenses, i.e., Apache 2.0 for most

Table 19: Mean squared error for each weather variable for selected pressure levels, the cumulative error for each atmospheric variable over all pressure levels, and the cumulative error over all variables and pressure levels. The selected pressure levels align with the evaluated levels of WeatherBench2 [Rasp et al., 2024]. Persistence is a basic weather forecasting model that provides a forecast by simply assuming that variable values remain constant, as they are in the input values. GraphCast refers to the GraphCast model proposed by Lam et al. [2023]. Table formatting k indicates a multiplicative factor of 10^3 while n indicates $10^{(-9)}$.

Pressure Level	Variable	GT	Persistence	GraphCast
All	All variables	179.629k	-	-
Surface	2-m temperature (2T)	7.572	7.123	0.068
	10-m u wind component (10U)	5.072	2.166	0.012
	10-m v wind component (10V)	6.102	3.266	0.013
	Mean sea level pressure (MSL)	102.551k	60.056k	240.832
	Total precipitation (TP)	0.009	714.517n	52.377n
500	Temperature (T)	2.751	1.120	0.007
	U component of wind (U)	15.026	6.658	0.048
	V component of wind (V)	27.003	12.988	0.053
	Geopotential (Z)	86.250k	48.637k	155.057
	Specific humidity (Q)	0.010	66.211n	1.090n
	Vertical wind speed (W)	0.032	6.242	0.050
700	Temperature (T)	2.406	1.051	0.006
	U component of wind (U)	8.716	3.951	0.025
	V component of wind (V)	14.156	6.754	0.027
	Geopotential (Z)	51.669k	32.773k	141.296
	Specific humidity (Q)	0.009	250.556n	3.304n
	Vertical wind speed (W)	0.024	3.352	0.027
850	Temperature (T)	2.832	1.351	0.009
	U component of wind (U)	9.151	4.015	0.022
	V component of wind (V)	12.289	6.565	0.023
	Geopotential (Z)	51.542k	32.453k	139.716
	Specific humidity (Q)	0.010	354.058n	4.881n
	Vertical wind speed (W)	0.016	3.517	0.024
All	Temperature (T)	2.805	-	-
	U component of wind (U)	13.855	-	-
	V component of wind (V)	21.501	-	-
	Geopotential (Z)	77.020k	-	-
	Specific humidity (Q)	0.010	-	-
	Vertical wind speed (W)	0.018	-	-

datasets (including WeatherBench2), MIT for SAT instances, and GPL for AClib. Regarding social networks, we report that the original BlueSky data are hosted at <https://zenodo.org/records/11082879> under the Creative Commons Attribution 4.0 International License. The owners of such data may update these records to comply with users’ “Right to Erasure”, and we are in the process of implementing a system to update our dataset consistently. **GRAPHBENCH** is continuously updated with new datasets, and data is hosted on institutional servers and public repositories for persistent access.

5. Automated hyperparameter optimization

GRAPHBENCH also integrates automated hyperparameter optimization (HPO), which aims to easily tune new models, improve performance, and enhance reproducibility. The hyperparameter optimization in **GRAPHBENCH** is based on the SMAC3 [Lindauer et al., 2022] package, which utilizes multi-fidelity scheduling. This approach evaluates many configurations on lower budgets and eliminates those with poor performance. As graph learning approaches are expensive to train, this approach enables the saving of costly resources. Additionally, SMAC3 uses a surrogate model to propose new configurations, thereby leveraging prior experience and further reducing computational load. Due to limited computational resources, we were unable to run HPO on all datasets and domains. To showcase the effectiveness of the automated hyperparameter optimization included in **GRAPHBENCH**, we tuned the GIN model on the **SMALL** SAT dataset with VG. We set the total optimization budget to 150 evaluations, varying fidelity over training gradient steps between 1 000 and 100 000. The used configuration space is shown in Table 20, and the results are presented in Table 21. We observe a 7.3% reduction in RMSE between the manually tuned and automatically tuned versions, demonstrating that automated HPO in **GRAPHBENCH** can improve model performance.

Table 20: GIN Configuration space used in the hyperparameter optimization experiment.

Hyperparameter	Range
Learning rate	[1e-6, 0.1]
Weight decay	[1e-8, 0.1]
Warmup iterations	[1 000, 20 000]
Dropout	[0.0, 0.5]

Table 21: **SAT Solving.** RMSE (\log_{10} time) for performance prediction on **SMALL** SAT instances. We compare the manually tuned version of GIN to the automatically tuned version. Lower is better.

Solver	Method	VG
KISSAT	GIN	1.36 ± 0.15
	GIN (tuned)	1.26 ± 0.03

6. Conclusion and outlook

In this work, we introduce **GRAPHBENCH**, a next-generation benchmarking suite that addresses the fragmentation and limitations of existing graph learning benchmarks. By unifying diverse domains—social sciences, hardware design, reasoning and optimization, and earth systems—into a single standardized framework, **GRAPHBENCH** enables fair and reproducible comparisons across a wide range of graph tasks. Our benchmarks cover node-, edge-, and graph-level prediction as well as generative settings, with realistic splits, relevant metrics, and explicit tests for out-of-distribution generalization. Comprehensive baselines with modern MPNNs and GTs provide strong reference points for future work. Results reveal persistent challenges—including temporal distribution shifts, scaling to large graphs, and capturing domain-specific structures. By offering principled datasets, consistent evaluation, and robust baselines, **GRAPHBENCH** aims to drive the development of more generalizable and practically relevant graph learning methods.

Vision for **GRAPHBENCH** *Looking ahead, we envision **GRAPHBENCH** as a living benchmark—continually expanding to include new domains, tasks, and evaluation paradigms, and serving as a catalyst for progress in both fundamental research and impactful real-world applications of graph machine learning.* In addition, we aim to extend **GRAPHBENCH** so that it offers support for training the next-generation of multi-modal graph foundation models.

References

N. Alamgir, S. Nejati, and C. Bright. SHA-256 collision attack with programmatic SAT. In *Workshop on Practical Aspects of Automated Reasoning (PAAR) and Satisfiability Checking and Symbolic Computation Workshop (SC-Square), adjunct to (IJCAR 2024)*, 2024.

R. Albert and A.-L. Barabási. Statistical mechanics of complex networks. *Reviews of modern physics*, (1), 2002.

F. Alet, I. Price, A. El-Kadi, D. Masters, S. Markou, T. R. Andersson, J. Stott, R. Lam, M. Willson, A. Sanchez-Gonzalez, and P. Battaglia. Skillful joint probabilistic weather forecasting from marginals. *ArXiv preprint*, 2025.

C. Ansótegui, J. Giráldez-Cru, and J. Levy. The community structure of SAT formulas. In *Proceedings of the International Conference on Theory and Applications of Satisfiability Testing (SAT)*, 2012.

V. Arvind, F. Fuhlbrück, J. Köbler, and O. Verbitsky. On weisfeiler-leman invariance: Subgraph counts and related graph properties. *Journal of Computer and System Sciences*, 2020.

T. Balyo, M. J. H. Heule, and M. Järvisalo. SAT competition 2016: Recent developments. In *Proceedings of the AAAI Conference on Artificial Intelligence*, 2017.

A. Bansal, D. Stoll, M. Janowski, A. Zela, and F. Hutter. Jahs-bench-201: A foundation for research on joint architecture and hyperparameter search. In *Proceedings of Advances in Neural Information Processing Systems NeurIPS*, 2022.

A.-L. Barabási and R. Albert. Emergence of scaling in random networks. *science*, (5439), 1999.

P. Bauer, A. Thorpe, and G. Brunet. The quiet revolution of numerical weather prediction. *Nature*, (7567), 2015.

G. Bazhenov, O. Platonov, and L. Prokhorenkova. Graphland: Evaluating graph machine learning models on diverse industrial data. *arXiv preprint*, 2025.

M. Bechler-Speicher, B. Finkelshtein, F. Frasca, L. Müller, J. Tönshoff, A. Sirauidin, V. Zaverkin, M. M. Bronstein, M. Niepert, B. Perozzi, M. Galkin, and C. Morris. Position: Graph learning will lose relevance due to poor benchmarks. *ArXiv preprint*, 2025.

Y. Bengio, A. Lodi, and A. Prouvost. Machine learning for combinatorial optimization: A methodological tour d'horizon. *European Journal of Operational Research*, (2), 2021.

B. Bevilacqua, K. Nikiforou, B. Ibarz, I. Bica, M. Paganini, C. Blundell, J. Mitrovic, and P. Velickovic. Neural algorithmic reasoning with causal regularisation. In *Proceedings of the International Conference on Machine Learning ICML*, Proceedings of Machine Learning Research, 2023.

K. Bi, L. Xie, H. Zhang, X. Chen, X. Gu, and Q. Tian. Pangu-weather: A 3d high-resolution model for fast and accurate global weather forecast. *ArXiv preprint*, 2022.

A. Biere, M. Heule, H. van Maaren, and T. Walsh. *Handbook of Satisfiability*. Frontiers in Artificial Intelligence and Applications. 2009.

A. Biere, K. Heljanko, and S. Wieringa. Aiger 1.9 and beyond, 2011.

A. Biere, M. Heule, H. v. Maaren, and T. Walsh. *Handbook of Satisfiability - Second Edition*. 2021.

A. Biere, M. Fleury, and F. Pollitt. Cadical_vivinst, isasat, gimsatul, kissat, and tabularasat entering the sat competition 2023. In *Proceedings of SAT Competition 2023*, 2023.

A. Biere, T. Faller, K. Fazekas, M. Fleury, N. Froleyks, and F. Pollitt. CaDiCaL, Gimsatul, IsaSAT and Kissat entering the SAT Competition 2024. In *Proceedings of SAT Competition 2024*, 2024.

B. Bischl, P. Kerschke, L. Kotthoff, M. Lindauer, Y. Malitsky, A. Fréchette, H. H. Hoos, F. Hutter, K. Leyton-Brown, K. Tierney, and J. Vanschoren. Aslib: A benchmark library for algorithm selection. *Artificial Intelligence*, 2016.

C. Bodnar. Aurora: A foundation model of the atmosphere. In *AGU Fall Meeting Abstracts*, 2024.

B. Bogaerts, J. Nordström, A. Oertel, and C. U. Yıldırımoglu. Breakid-kissat in sat competition 2023 (system description). In *Proceedings of SAT Competition 2023*, 2023.

B. Bogaerts, J. Nordström, A. Oertel, and D. Vandesande. BreakID-kissat in SAT Competition 2024 (System Description). In *Proceedings of SAT Competition 2024*, 2024.

M. Böther, O. Kißig, M. Taraz, S. Cohen, K. Seidel, and T. Friedrich. What's wrong with deep learning in tree search for combinatorial optimization. In *Proceedings of the International Conference on Learning Representations ICLR*, 2022.

W. Bounsi, B. Ibarz, A. Dudzik, J. B. Hamrick, L. Markeeva, A. Vitvitskyi, R. Pascanu, and P. Velickovic. Transformers meet neural algorithmic reasoners. *arXiv preprint*, 2024.

I. Boussaïd, J. Lepagnot, and P. Siarry. A survey on optimization metaheuristics. *Information sciences*, 2013.

R. Brayton and A. Mishchenko. Abc: An academic industrial-strength verification tool. In *Proceedings of the International Conference on Computer Aided Verification CAV*. Springer, 2010.

L. Breiman. Random forests. *Machine Learning*, (1), 2001.

R. Brummayer, F. Lonsing, and A. Biere. Automated testing and debugging of SAT and QBF solvers. In *Proceedings of the International Conference on Theory and Applications of Satisfiability Testing SAT*, Lecture Notes in Computer Science, 2010.

Q. Cappart, D. Chételat, E. B. Khalil, A. Lodi, C. Morris, and P. Velickovic. Combinatorial optimization and reasoning with graph neural networks. In *Proceedings of the International Joint Conference on Artificial Intelligence IJCAI*, 2021.

M. Caramia and P. Dell’Olmo. k -insertions graphs: a proposal of a new class of benchmarks. Manuscript, 2002a.

M. Caramia and P. Dell’Olmo. k -fullins graphs: a proposal of a new class of benchmarks. Manuscript, 2002b.

A. Carballo-Castro, M. Madeira, Y. Qin, D. Thanou, and P. Frossard. Generating directed graphs with dual attention and asymmetric encoding. *ArXiv preprint*, 2025.

T. Chen and C. Guestrin. Xgboost: A scalable tree boosting system. In *Proceedings of the ACM SIGKDD International Conference on Knowledge Discovery and Data Mining*, 2016.

Z. Chen, J. Liu, X. Wang, and W. Yin. On representing mixed-integer linear programs by graph neural networks. In *Proceedings of the International Conference on Learning Representations ICLR*, 2023.

Z. Chen, J. Liu, X. Chen, X. Wang, and W. Yin. Rethinking the capacity of graph neural networks for branching strategy. In *Proceedings of Advances in Neural Information Processing Systems NeurIPS*, 2024.

V. Chvátal. Coloring the queen graphs, 2004. URL <http://www.cs.concordia.ca/~chvatal/queengraphs.html>. Web repository.

S. A. Cook. The complexity of theorem-proving procedures. *ACM Symposium on Theory of Computing (STOC)*, 1971.

T. H. Cormen, C. E. Leiserson, R. L. Rivest, and C. Stein. *Introduction to Algorithms, 3rd Edition*. 2009. ISBN 978-0-262-03384-8.

C. Coupette, J. Wayland, E. Simons, and B. Rieck. No metric to rule them all: Toward principled evaluations of graph-learning datasets. In *Proceedings of the International Conference on Machine Learning ICML*, 2025.

C. Diao and R. Loynd. Relational attention: Generalizing transformers for graph-structured tasks. In *Proceedings of the International Conference on Learning Representations ICLR*, 2023.

A. Diehl, S. Bruckner, M. E. Gröller, C. Delrieux, and C. Saulo. Visual trend analysis in weather forecast. In *Proceedings of the International Conference on Information Visualisation*, 2013.

V. P. Dwivedi, C. K. Joshi, T. Laurent, Y. Bengio, and X. Bresson. Benchmarking graph neural networks. *arXiv preprint*, 2020.

V. P. Dwivedi, A. T. Luu, and Y. Bengio. Graph neural networks with adaptive message passing for long-range dependencies. In *Proceedings of Advances in Neural Information Processing Systems NeurIPS*, 2022a.

V. P. Dwivedi, A. T. Luu, T. Laurent, Y. Bengio, and X. Bresson. Graph neural networks with learnable structural and positional representations. In *Proceedings of the International Conference on Learning Representations ICLR*, 2022b.

K. Eggensperger, F. Hutter, H. H. Hoos, and K. Leyton-Brown. Efficient benchmarking of hyperparameter optimizers via surrogates. In *Proceedings of the AAAI Conference on Artificial Intelligence*, 2015.

K. Eggensperger, M. Lindauer, and F. Hutter. Pitfalls and best practices in algorithm configuration. *Journal of Artificial Intelligence Research*, 2019.

P. Erdős and A. Rényi. On the evolution of random graphs. *Publ. Math. Inst. Hungar. Acad. Sci*, 1960.

B. Estermann, L. A. Lanzendorfer, Y. Niedermayr, and R. Wattenhofer. PUZZLES: A benchmark for neural algorithmic reasoning. In *Proceedings of the Advances in Neural Information Processing Systems NeurIPS*, 2024.

A. Failla and G. Rossetti. “i’m in the bluesky tonight”: Insights from a year worth of social data. *PLoS ONE*, (11), 2024.

L. Fan, W. Hua, L. Li, H. Ling, and Y. Zhang. Nphardeval: Dynamic benchmark on reasoning ability of large language models via complexity classes. In *Proceedings of the Annual Meeting of the Association for Computational Linguistics (Volume 1: Long Papers)*, 2024a.

S. Fan, N. Cao, S. Zhang, J. Li, X. Guo, and X. Zhang. From specification to topology: Automatic power converter design via reinforcement learning. *IEEE/ACM International Conference On Computer Aided Design (ICCAD)*, 2021.

S. Fan, H. Lu, S. Zhang, N. Cao, X. Zhang, and J. Li. Graph-transformer-based surrogate model for accelerated converter circuit topology design. In *Proceedings of the ACM/IEEE Design Automation Conference*, 2024b.

M. Fey and J. E. Lenssen. Fast graph representation learning with pytorch geometric. *arXiv preprint*, 2019.

M. Fey, J. Sunil, A. Nitta, R. Puri, M. Shah, B. Stojanović, R. Bendias, A. Barghi, V. Kocijan, Z. Zhang, X. He, J. E. Lenssen, and J. Leskovec. Pyg 2.0: Scalable learning on real world graphs. In *Proceedings of the Temporal Graph Learning Workshop adjunct to KDD*, 2025.

N. Froleyks, M. Heule, A. Iser, M. Järvisalo, and M. Suda. SAT competition 2020. *Artificial Intelligence*, 2021.

E. Gansner, E. Koutsofios, and S. North. Drawing graphs with dot, 2006.

Y. Gao. Kissat MAB prop in SAT Competition 2023. In *Proceedings of SAT Competition 2023*, 2023.

Y. Gao, H. Wu, R. Shu, H. Dong, F. Xu, R. R. Chen, Y. Yan, Q. Wen, X. Hu, K. Wang, J. Wu, Q. Li, H. Xiong, and X. Huang. Oneforecast: a universal framework for global and regional weather forecasting. In *Proceedings of the International Conference on Machine Learning ICML*, 2025.

M. Gasse, S. Bowly, Q. Cappart, J. Charfreitag, L. Charlin, D. Chételat, A. Chmiela, J. Dumouchelle, A. Gleixner, A. M. Kazachkov, E. Khalil, P. Lichocki, A. Lodi, M. Lubin, C. J. Maddison, C. Morris, D. J. Papageorgiou, A. Parjadis, S. Pokutta, A. Prouvost, L. Scavuzzo, G. Zarpellon, L. Yang, S. Lai, A. Wang, X. Luo, X. Zhou, H. Huang, S. Shao, Y. Zhu, D. Zhang, T. Quan, Z. Cao, Y. Xu, Z. Huang, S. Zhou, B. Chen, M. He, H. Hao, Z. Zhang, Z. An, and M. Kun. The machine learning for combinatorial optimization competition (ml4co): Results and insights. In *Proceedings of Advances in Neural Information Processing Systems NeurIPS, Competitions and Demonstrations Track*, 2022.

J. Gilmer, S. S. Schoenholz, P. F. Riley, O. Vinyals, and G. E. Dahl. Neural message passing for quantum chemistry. In *Proceedings of the International Conference on Machine Learning ICML, Proceedings of Machine Learning Research*, 2017.

J. Giráldez-Cru and J. Levy. Generating SAT instances with community structure. *Artificial Intelligence*, 2016.

A. V. Goldberg and R. E. Tarjan. A new approach to the maximum flow problem. In *Proceedings of the Annual ACM Symposium on Theory of Computing*, 1986. ISBN 0897911938.

A. Goldie, A. Mirhoseini, and J. Dean. That chip has sailed: A critique of unfounded skepticism around ai for chip design. *arXiv preprint*, 2024.

C. Gomes and D. Shmoys. Completing quasigroups or latin squares: A structured graph coloring problem. In *Proceedings of the Computational Symposium on Graph Coloring and Generalizations*, 2002.

C. P. Gomes, H. Kautz, A. Sabharwal, and B. Selman. Satisfiability solvers. *Handbook of Knowledge Representation*, 2008.

F. Gonard, M. Schoenauer, and M. Sebag. ASAP.V2 and ASAP.V3: sequential optimization of an algorithm selector and a scheduler. In *Open Algorithm Selection Challenge 2017*, Proceedings of Machine Learning Research, 2017.

Gurobi Optimization, LLC. Gurobi Optimizer Reference Manual, 2024.

A. Haberlandt and H. Green. Sbva-cadical and sbva-kissat: Structured bounded variable addition. In *Proceedings of SAT Competition 2023*, 2023.

A. Hagberg and D. Conway. Networkx: Network analysis with python. *URL: <https://networkx.github.io>*, 2020.

W. L. Hamilton, Z. Ying, and J. Leskovec. Inductive representation learning on large graphs. In *Proceedings of Advances in Neural Information Processing Systems NeurIPS*, 2017.

F. He, T. Liu, and D. Tao. Why resnet works? residuals generalize. *IEEE transactions on neural networks and learning systems*, (12), 2020.

D. Hendrycks and K. Gimpel. Bridging nonlinearities and stochastic regularizers with gaussian error linear units. *arXiv preprint*, 2016.

M. J. H. Heule, M. Järvisalo, and M. Suda. SAT competition 2018. *Journal on Satisfiability, Boolean Modeling and Computation*, (1), 2019.

P. W. Holland, K. B. Laskey, and S. Leinhardt. Stochastic blockmodels: First steps. *Social networks*, (2), 1983.

P. Holme and B. J. Kim. Growing scale-free networks with tunable clustering. *Physical review E*, (2), 2002.

J. E. Hopcroft and R. M. Karp. An $n^{5/2}$ algorithm for maximum matchings in bipartite graphs. *SIAM Journal on computing*, (4), 1973.

W. Hu, M. Fey, M. Zitnik, Y. Dong, H. Ren, B. Liu, M. Catasta, and J. Leskovec. Open graph benchmark: Datasets for machine learning on graphs. In *Proceedings of Advances in Neural Information Processing Systems NeurIPS*, 2020a.

W. Hu, B. Liu, J. Gomes, M. Zitnik, P. Liang, V. S. Pande, and J. Leskovec. Strategies for pre-training graph neural networks. In *8th International Conference on Learning Representations, ICLR*, 2020b.

W. Hu, M. Fey, H. Ren, M. Nakata, Y. Dong, and J. Leskovec. Ogb-lsc: A large-scale challenge for machine learning on graphs. *arXiv preprint*, 2021.

F. Hutter, L. Kotthoff, H. H. Hoos, and K. Leyton-Brown. Algorithm runtime prediction: Methods & evaluation. *Artificial Intelligence*, 2014a.

F. Hutter, M. López-Ibáñez, C. Fawcett, M. Lindauer, H. H. Hoos, K. Leyton-Brown, and T. Stützle. Aclib: A benchmark library for algorithm configuration. In *Proceedings of the International Conference on Learning and Intelligent Optimization, Revised Selected Papers*, Lecture Notes in Computer Science, 2014b.

F. Hutter, L. Xu, H. H. Hoos, and K. Leyton-Brown. Algorithm runtime prediction: Methods & evaluation. *Artificial Intelligence*, 2014c.

B. Ibarz, V. Kurin, G. Papamakarios, K. Nikiforou, M. Bennani, R. Csordás, A. J. Dudzik, M. Bosnjak, A. Vitvitskyi, Y. Rubanova, A. Deac, B. Bevilacqua, Y. Ganin, C. Blundell, and P. Velickovic. A generalist neural algorithmic learner. In *Proceedings of the Learning on Graphs Conference*, Proceedings of Machine Learning Research, 2022.

R. Ilango, B. Loff, and I. C. Oliveira. Np-hardness of circuit minimization for multi-output functions. CCC '20, Dagstuhl, DEU, 2020. Schloss Dagstuhl–Leibniz-Zentrum fuer Informatik. ISBN 9783959771566. doi: 10.4230/LIPIcs.CCC.2020.22. URL <https://doi.org/10.4230/LIPIcs.CCC.2020.22>.

A. Iser and C. Jabs. Global benchmark database. In *Proceedings of the International Conference on Theory and Applications of Satisfiability Testing SAT*, LIPIcs, 2024.

A. Jabrayilov and P. Mutzel. New integer linear programming models for the vertex coloring problem. In *Proceedings of LATIN: Theoretical Informatics: Latin American Symposium*, 2018.

A. B. Kahn. Topological sorting of large networks. *Commun. ACM*, 5(11):558–562, 1962. doi: 10.1145/368996.369025. URL <https://doi.org/10.1145/368996.369025>.

L. Kaiser and I. Sutskever. Neural gpus learn algorithms. In *Proceedings of the International Conference on Learning Representations ICLR*, 2016.

N. Karalias and A. Loukas. Erdos goes neural: an unsupervised learning framework for combinatorial optimization on graphs. In *Proceedings of Advances in Neural Information Processing Systems NeurIPS*, 2020.

R. M. Karp. Reducibility among combinatorial problems. In *Complexity of Computer Computations*. 1972.

H. Kautz and B. Selman. Pushing the envelope: Planning, propositional logic, and stochastic search. In *Proceedings of the AAAI Conference on Artificial Intelligence*, 1996.

R. Keisler. Forecasting global weather with graph neural networks. *arXiv preprint*, 2022.

P. Kerschke, L. Kotthoff, J. Bossek, H. H. Hoos, and H. Trautmann. Leveraging TSP solver complementarity through machine learning. *Evolutionary Computation*, (4), 2018.

B. Korte and J. Vygen. *Combinatorial Optimization: Theory and Algorithms*. 5th edition, 2012.

L. Kotthoff. LLAMA: leveraging learning to automatically manage algorithms. *arXiv preprint*, 2013.

L. Kou, G. Markowsky, and L. Berman. A fast algorithm for steiner trees. *Acta informatica*, (2), 1981.

J. B. Kruskal. On the shortest spanning subtree of a graph and the traveling salesman problem. *Proceedings of the American Mathematical society*, (1), 1956.

R. Lam, A. Sanchez-Gonzalez, M. Willson, P. Wirnsberger, M. Fortunato, F. Alet, S. Ravuri, T. Ewalds, Z. Eaton-Rosen, W. Hu, A. Merose, S. Hoyer, G. Holland, O. Vinyals, J. Stott, A. Pritzel, S. Mohamed, and P. Battaglia. Learning skillful medium-range global weather forecasting. *Science*, (6677), 2023.

S. Lamm, P. Sanders, C. Schulz, D. Strash, and R. F. Werneck. Finding near-optimal independent sets at scale. In *Proceedings of the Workshop on Algorithm Engineering and Experiments, ALENEX*, 2016.

J. Leskovec and R. Sosic. Snap: A general purpose network analysis and graph mining library. *arXiv preprint*, 2016.

R. Lewis and G. Palmer. Gcol: A high-performance python library for graph colouring. *The Journal of Open Source Software*, (108), 2025.

H. Li, C. Peng, C. Xu, and Z. Yang. Open-book neural algorithmic reasoning. In *Proceedings of Advances in Neural Information Processing Systems NeurIPS*, 2024a.

M. Li, V. Shitole, E. Chien, C. Man, Z. Wang, Y. Zhang, T. Krishna, and P. Li. Layerdag: A layerwise autoregressive diffusion model for directed acyclic graph generation. In *Proceedings of the Will Synthetic Data Finally Solve the Data Access Problem? workshop, adjunct to ICLR*, 2025a.

S. Li, C.-M. Li, M. Luo, J. Coll, M. S. Cherif, D. Habet, and F. Manyà. Esa solvers, kissat mab binary and amsat in sat competition 2024. In *Proceedings of SAT Competition 2024*, 2024b.

W. Li, R. Li, Y. Ma, S. O. Chan, D. Pan, and B. Yu. Rethinking graph neural networks for the graph coloring problem. *arXiv preprint*, 2022.

X. Li, X. Li, L. Chen, X. Zhang, M. Yuan, and J. Wang. Circuit transformer: A transformer that preserves logical equivalence. In *Proceedings of the International Conference on Learning Representations ICLR*, 2025b.

Z. Li, J. Guo, and X. Si. G4satbench: Benchmarking and advancing SAT solving with graph neural networks. *Transactions on Machine Learning Research*, 2024c.

M. Lindauer, H. H. Hoos, F. Hutter, and T. Schaub. Autofolio: An automatically configured algorithm selector. *Journal of Artificial Intelligence Research*, 2015.

M. Lindauer, J. N. van Rijn, and L. Kotthoff. The algorithm selection competitions 2015 and 2017. *Artificial Intelligence*, 2019.

M. Lindauer, K. Eggensperger, M. Feurer, A. Biedenkapp, D. Deng, C. Benjamins, T. Ruhkopf, R. Sass, and F. Hutter. SMAC3: A versatile bayesian optimization package for hyperparameter optimization. *J. Mach. Learn. Res.*, 2022.

J. Liu, J. Zhang, and Y. Sun. Kissat_mab-dc in sat competition 2024. In *Proceedings of SAT Competition 2024*, 2024.

Y.-C. Lu, S. S. K. Pentapati, L. Zhu, K. Samadi, and S. K. Lim. Tp-gnn: A graph neural network framework for tier partitioning in monolithic 3d ics. *Proceedings of the ACM/IEEE Design Automation Conference (DAC)*, 2020.

S. Mahdavi, K. Swersky, T. Kipf, M. Hashemi, V. Thrampoulidis, and R. Liao. Towards better out-of-distribution generalization of neural algorithmic reasoning tasks. *Transactions on Machine Learning Research*, 2023.

U. Mallappa, H. Mostafa, M. Galkin, M. Phiellipp, and S. Majumdar. Floorset-a vlsi floorplanning dataset with design constraints of real-world socs. In *Proceedings of the IEEE/ACM International Conference on Computer-Aided Design ICCAD*, 2024.

T. McConaghy, P. Palmers, M. Steyaert, and G. G. E. Gielen. Trustworthy genetic programming-based synthesis of analog circuit topologies using hierarchical domain-specific building blocks. *IEEE Transactions on Evolutionary Computation*, 2011.

Y. Min, F. Wenkel, M. Perlmutter, and G. Wolf. Can hybrid geometric scattering networks help solve the maximum clique problem? In *Proceedings of Advances in Neural Information Processing Systems NeurIPS*, 2022.

A. Mirhoseini, A. Goldie, M. Yazgan, J. W. Jiang, E. M. Songhori, S. Wang, Y. Lee, E. Johnson, O. Pathak, A. Nazy, J. Pak, A. Tong, K. Srinivasa, W. Hang, E. Tuncer, Q. V. Le, J. Laudon, R. Ho, R. Carpenter, and J. Dean. A graph placement methodology for fast chip design. *Nature*, (7862), 2021.

A. Mishchenko and Y. Miyasaka. Problems and results of iwls 2023 programming contest, 2023.

A. Mishchenko, S. Chatterjee, R. Jiang, and R. K. Brayton. Fraigs: A unifying representation for logic synthesis and verification. Technical report, ERL Technical Report, 2005.

K. Mizuno and S. Nishihara. Toward systematic generation of 3col instances based on minimal unsolvable structures. *Electronics and Communications in Japan (Part III: Fundamental Electronic Science)*, (12), 2007.

K. Mizuno and S. Nishihara. Constructive generation of very hard 3-colorability instances. *Discrete Applied Mathematics*, (2), 2008.

C. Morris, N. M. Kriege, F. Bause, K. Kersting, P. Mutzel, and M. Neumann. TUDataset: A collection of benchmark datasets for learning with graphs. *arXiv preprint*, 2020.

N. Moshiri. The dual-barab\`asi-albert model. *arXiv preprint*, 2018.

L. Müller and C. Morris. Aligning transformers with weisfeiler-leman. In *Proceedings of the International Conference on Machine Learning ICML*, 2024.

L. Müller, M. Galkin, C. Morris, and L. Rampásek. Attending to graph transformers. *Transactions on Machine Learning Research*, 2024a.

L. Müller, D. Kusuma, B. Bonet, and C. Morris. Towards principled graph transformers. In *Proceedings of Advances in Neural Information Processing Systems (NeurIPS)*, 2024b.

A. Nath and A. Kuhnle. A benchmark for maximum cut: Towards standardization of the evaluation of learned heuristics for combinatorial optimization. *Transactions on Machine Learning Research*, 2024.

S. Nejati, J. H. Liang, C. H. Gebotys, K. Czarnecki, and V. Ganesh. Adaptive restart and cegar-based solver for inverting cryptographic hash functions. In *Proceedings of the International Conference on Verified Software. Theories, Tools, and Experiments VSTTE, Revised Selected Papers*, Lecture Notes in Computer Science, 2017.

P. Nenzi and H. Vogt. *Ngspice User's Manual, Version 23*, 2011. URL <https://pkgs.fedoraproject.org/repo/extras/ngspice/ngspice23-manual.pdf/eb0d68eb463a41a0571757a00a5b9f9d/ngspice23-manual.pdf>. Accessed: 2025-09-23.

M. E. J. Newman. *Networks: An Introduction*. 2010. ISBN 9780199206650.

M. E. J. Newman and D. J. Watts. Renormalization group analysis of the small-world network model. *Physics Letters A*, (4-6), 1999.

E. Nudelman, K. Leyton-Brown, H. H. Hoos, A. Devkar, and Y. Shoham. Understanding Random SAT: Beyond the Clauses-to-Variables Ratio. In *Proceedings of International Conference on Principles and Practice of Constraint Programming CP*, 2004.

J. Oskarsson, T. Landelius, M. P. Deisenroth, and F. Lindsten. Probabilistic weather forecasting with hierarchical graph neural networks. In *Proceedings of Advances in Neural Information Processing Systems NeurIPS*, 2024.

S. Ou, Q. Yang, and J. Liu. The global production pattern of the semiconductor industry: an empirical research based on trade network. *Humanities and Social Sciences Communications*, 11(1):750, 2024. ISSN 2662-9992. doi: 10.1057/s41599-024-03253-5. URL <https://doi.org/10.1057/s41599-024-03253-5>.

V. T. Paschos. *Applications of combinatorial optimization*. 2014.

I. Price, A. Sanchez-Gonzalez, F. Alet, T. R. Andersson, A. El-Kadi, D. Masters, T. Ewalds, J. Stott, S. Mohamed, P. Battaglia, R. Lam, and M. Willson. Gencast: Diffusion-based ensemble forecasting for medium-range weather. *arXiv preprint*, 2023.

R. Qiu, Z. Sun, and Y. Yang. DIMES: A differentiable meta solver for combinatorial optimization problems. In *Proceedings of Advances in Neural Information Processing Systems NeurIPS*, 2022.

S. Rai, W. L. Neto, Y. Miyasaka, X. Zhang, M. Yu, Q. Yi, M. Fujita, G. B. Manske, M. F. Pontes, L. S. Da Rosa, et al. Logic synthesis meets machine learning: Trading exactness for generalization. In *2021 Design, Automation & Test in Europe Conference & Exhibition (DATE)*, pages 1026–1031. IEEE, 2021.

K. Ramar and T. Mirnalinee. A semantic web for weather forecasting systems. In *Proceedings of the International Conference on Recent Trends in Information Technology*. IEEE, 2014.

S. Rasp, P. D. Dueben, S. Scher, J. A. Weyn, S. Mouatadid, and N. Thuerey. Weatherbench: a benchmark data set for data-driven weather forecasting. *Journal of Advances in Modeling Earth Systems*, (11), 2020.

S. Rasp, S. Hoyer, A. Merose, I. Langmore, P. Battaglia, T. Russell, A. Sanchez-Gonzalez, V. Yang, R. Carver, S. Agrawal, M. Chantry, Z. B. Bouallegue, P. Dueben, C. Bromberg, J. Sisk, L. Barrington, A. Bell, and F. Sha. Weatherbench 2: A benchmark for the next generation of data-driven global weather models. *Journal of Advances in Modeling Earth Systems*, (6), 2024.

J. E. Reeves and R. E. Bryant. Preprocessors prelearn and reencode entering the sat competition 2023. In *Proceedings of SAT Competition 2023*, 2023.

M. Reichstein, G. Camps-Valls, B. Stevens, M. Jung, J. Denzler, N. Carvalhais, and F. Prabhat. Deep learning and process understanding for data-driven earth system science. *Nature*, (7743), 2019.

J. R. Rice. The algorithm selection problem. *Advances in Computers*, 1976.

G. Rodionov and L. Prokhorenkova. Neural algorithmic reasoning without intermediate supervision. In *Proceedings of Advances in Neural Information Processing Systems NeurIPS*, 2023.

R. A. Rossi and N. K. Ahmed. The network data repository with interactive graph analytics and visualization. In *Proceedings of the AAAI Conference on Artificial Intelligence*, 2015.

O. Roussel. Controlling a solver execution with the runsolver tool. *Journal on Satisfiability, Boolean Modeling and Computation*, (4), 2011.

B. Rozemberczki, C. Allen, and R. Sarkar. Multi-scale attributed node embedding. *ArXiv preprint*, 2021.

S. Sanokowski, S. Hochreiter, and S. Lehner. A diffusion model framework for unsupervised neural combinatorial optimization. In *Proceedings of the International Conference on Machine Learning ICML*, 2024.

V. Satopaa, J. R. Albrecht, D. E. Irwin, and B. Raghavan. Finding a "needle" in a haystack: Detecting knee points in system behavior. In *Proceedings of the IEEE International Conference on Distributed Computing Systems ICDCS Workshops*, 2011.

F. Scarselli, M. Gori, A. C. Tsoi, M. Hagenbuchner, and G. Monfardini. The graph neural network model. *IEEE Transactions on Neural Networks*, (1), 2009.

D. Selsam, M. Lamm, B. Bünz, P. Liang, L. de Moura, and D. L. Dill. Learning a SAT solver from single-bit supervision. In *Proceedings of the International Conference on Learning Representations ICLR*, 2019.

H. Shavit. Algorithm selection for SAT using graph neural networks. Master's thesis, Leiden University, 2023.

H. Shavit and H. H. Hoos. Revisiting SATzilla Features in 2024. In *Proceedings of the International Conference on Theory and Applications of Satisfiability Testing SAT*, 2024.

H. Shavit and H. H. Hoos. hadarshavit/asf: v0.1.0, in progress. URL <https://github.com/hadarshavit/asf>.

H. Sun, E. K. Guha, and H. Dai. Annealed training for combinatorial optimization on graphs. *arXiv preprint*, 2022.

Z. Sun and Y. Yang. DIFUSCO: graph-based diffusion solvers for combinatorial optimization. In *Proceedings of Advances in Neural Information Processing Systems NeurIPS*, 2023.

R. K. Tchinda and C. T. Djamegni. hkis, ukissatinc, pakisinc and pahkis in the sat competition 2023. In *Proceedings of SAT Competition 2023*, 2023.

J. Toenshoff, M. Ritzert, H. Wolf, and M. Grohe. Graph neural networks for maximum constraint satisfaction. *Frontiers in artificial intelligence*, 2021.

J. Tönshoff and M. Grohe. Learning from algorithm feedback: One-shot SAT solver guidance with gnns. *ArXiv preprint*, 2025.

J. Tönshoff, B. Kisín, J. Lindner, and M. Grohe. One model, any CSP: graph neural networks as fast global search heuristics for constraint satisfaction. In *Proceedings of the International Joint Conference on Artificial Intelligence IJCAI*, 2023.

D. Tsaras, X. Li, L. Chen, Z. Xie, and M. Yuan. Elf: Efficient logic synthesis by pruning redundancy in refactoring. In *Proceedings of the ACM/IEEE Design Automation Conference (DAC)*, pages 1–7. IEEE, 2025.

G. S. Tseitin. On the complexity of derivation in propositional calculus. In *Automation of reasoning: 2: Classical papers on computational logic 1967–1970*. 1983.

V. V. Vazirani. *Approximation Algorithms*. Springer, 2010.

P. Velickovic, L. Buesing, M. C. Overlan, R. Pascanu, O. Vinyals, and C. Blundell. Pointer graph networks. In *Proceedings of Advances in Neural Information Processing Systems NeurIPS*, 2020a.

P. Velickovic, R. Ying, M. Padovano, R. Hadsell, and C. Blundell. Neural execution of graph algorithms. In *Proceedings of the International Conference on Learning Representations ICLR*, 2020b.

P. Velickovic, A. P. Badia, D. Budden, R. Pascanu, A. Banino, M. Dashevskiy, R. Hadsell, and C. Blundell. The CLRS algorithmic reasoning benchmark. In *Proceedings of the International Conference on Machine Learning ICML*, Proceedings of Machine Learning Research, 2022.

C. Vignac, I. Krawczuk, A. Siraudin, B. Wang, V. Cevher, and P. Frossard. Digress: Discrete denoising diffusion for graph generation. In *Proceedings of the International Conference on Learning Representations ICLR*, 2023.

H. Wang, K. Wang, J. Yang, L. Shen, N. Sun, H.-S. Lee, and S. Han. Gcn-rl circuit designer: Transferable transistor sizing with graph neural networks and reinforcement learning. In *Proceedings of the ACM/IEEE Design Automation Conference (DAC)*, 2020.

W. Wang, Y. Hu, M. Tiwari, S. Khurshid, K. L. McMillan, and R. Miikkulainen. Neuroback: Improving CDCL SAT solving using graph neural networks. In *Proceedings of the International Conference on Learning Representations ICLR*, 2024.

F. Wenkel, S. Cantürk, S. Horoi, M. Perlmutter, and G. Wolf. Towards a general recipe for combinatorial optimization with multi-filter GNNs. In *Proceedings of the Learning on Graphs Conference*, 2024.

J. A. Weyn, D. R. Durran, and R. Caruana. Improving data-driven global weather prediction using deep convolutional neural networks on a cubed sphere. *Journal of Advances in Modeling Earth Systems*, (9), 2020.

R. Wille, D. Große, L. Teuber, G. W. Dueck, and R. Drechsler. RevLib: An online resource for reversible functions and reversible circuits. In *Proceedings of the International Symposium on Multiple-Valued Logic*, 2008. RevLib is available at <http://www.revlib.org>.

F. Wong, E. J. Zheng, J. A. Valeri, N. M. Donghia, M. N. Anahtar, S. Omori, A. Li, A. Cubillos-Ruiz, A. Krishnan, W. Jin, A. L. Manson, J. Friedrichs, R. Helbig, B. Hajian, D. K. Fiejtek, F. F. Wagner,

H. H. Soutter, A. M. Earl, J. M. Stokes, L. D. Renner, and J. J. Collins. Discovery of a structural class of antibiotics with explainable deep learning. *Nature*, 2023.

K. Xu, F. Boussemart, F. Hemery, and C. Lecoutre. Random constraint satisfaction: Easy generation of hard (satisfiable) instances. *Artificial Intelligence*, (8), 2007. ISSN 0004-3702.

K. Xu, J. Li, M. Zhang, S. S. Du, K. Kawarabayashi, and S. Jegelka. What can neural networks reason about? In *Proceedings of the International Conference on Learning Representations ICLR*, 2020.

L. Xu, F. Hutter, H. H. Hoos, and K. Leyton-Brown. Satzilla: Portfolio-based Algorithm Selection for SAT. *Journal of Artificial Intelligence Research*, 2008.

L. Xu, F. Hutter, J. Shen, H. H. Hoos, and K. Leyton-Brown. Satzilla2012: Improved algorithm selection based on cost-sensitive classification models. *Proceedings of SAT Challenge*, 2012.

Z. Yang, W. W. Cohen, and R. Salakhutdinov. Revisiting semi-supervised learning with graph embeddings. In *Proceedings of the International Conference on Machine Learning ICML*, JMLR Workshop and Conference Proceedings, 2016.

R. Ying, R. He, K. Chen, P. Eksombatchai, W. L. Hamilton, and J. Leskovec. Graph convolutional neural networks for web-scale recommender systems. In *Proceedings of the ACM SIGKDD International Conference on Knowledge Discovery & Data Mining, KDD*, 2018.

K. Yu, H. Zhao, Y. Huang, R. Yi, K. Xu, and C. Zhu. DISCO: Efficient diffusion solver for large-scale combinatorial optimization problems. *arXiv preprint*, 2024.

M. Zaheer, S. Kottur, S. Ravanbakhsh, B. Poczos, R. R. Salakhutdinov, and A. J. Smola. Deep sets. In *Advances in Neural Information Processing Systems*, volume 30, 2017.

W. Zaremba and I. Sutskever. Learning to execute. *arXiv preprint*, 2014.

D. Zhang, H. Dai, N. Malkin, A. C. Courville, Y. Bengio, and L. Pan. Let the flows tell: Solving graph combinatorial problems with gflownets. In *Proceedings of Advances in Neural Information Processing Systems NeurIPS*, 2023.

G. Zhang, H. He, and D. Katabi. Circuit-gnn: Graph neural networks for distributed circuit design. In *Proceedings of the International Conference on Machine Learning ICML*, Proceedings of Machine Learning Research, 2019.

Y. Zhang, H. Ren, and B. Khailany. Grannite: Graph neural network inference for transferable power estimation. *ACM/IEEE Design Automation Conference (DAC)*, 2020.

Z. Zhang, D. Chételat, J. Cotnareanu, A. Ghose, W. Xiao, H. Zhen, Y. Zhang, J. Hao, M. Coates, and M. Yuan. Grass: Combining graph neural networks with expert knowledge for SAT solver selection. In *Proceedings of the ACM SIGKDD Conference on Knowledge Discovery and Data Mining, KDD*, 2024.

Z. Zhao and L. Zhang. An automated topology synthesis framework for analog integrated circuits. *IEEE Transactions on Computer-Aided Design of Integrated Circuits and Systems*, 2020.

Z. Zheng, S. Huang, J. Zhong, Z. Shi, G. Dai, N. Xu, and Q. Xu. Deepgate4: Efficient and effective representation learning for circuit design at scale. In *Proceedings of the International Conference on Learning Representations ICLR*, 2025.

A. Dataset details

Here, we provide additional details on the datasets.

A.1. Social networks: BlueSky

More on metrics We assess model performance using two metrics: the coefficient of determination (R^2) and the Spearman correlation (ρ). Given a set of evaluation nodes $U \subset V$, reference engagement kind κ and prediction interval $\tau_{1,2}$, the former is defined as

$$R_{\kappa, \tau_{1,2}}^2 := 1 - \frac{\sum_{u \in U} (y_{\tau_{1,2}}^{\kappa, (u)} - \hat{y}^{\kappa, (u)})^2}{\sum_{u \in U} (y_{\tau_{1,2}}^{\kappa, (u)} - \bar{y}_{\tau_{1,2}}^{\kappa})^2},$$

where $\hat{y}^{\kappa, (u)}$ is the model’s prediction for engagement κ and user u and $\bar{y}_{\tau_{1,2}}^{\kappa}$ is the mean target value over U . This standard regression metric indicates the overall variance captured by the model, enabling assessment of its predictive accuracy relative to that of a trivial predictor. The Spearman correlation metric is defined, instead, as:

$$\sigma_{\kappa, \tau_{1,2}} := 1 - \frac{6 \cdot \sum_{u \in U} (R[y_{\tau_{1,2}}^{\kappa, (u)}] - R[\hat{y}^{\kappa, (u)}])^2}{n_U(n_U^2 - 1)},$$

where $n_U = |U|$ and expression $(R[y_{\tau_{1,2}}^{\kappa, (u)}] - R[\hat{y}^{\kappa, (u)}])$ evaluates the difference in the ranking of user $u \in U$ within either targets ($y_{\tau_{1,2}}^{\kappa}$) or model’s predictions (\hat{y}^{κ}). This measures how well predictions preserve the relative ordering of users by future engagement, and is not necessarily captured by accuracy metrics such as R^2 .

More details on the dataset

- *Graph structures:* Within a considered temporal split, we retain only nodes associated with posts in both $\tau_{0,1} = (t_0, t_1]$ and $\tau_{1,2} = (t_1, t_2]$. Only edges between the remaining nodes are kept, and further, arising isolated nodes are dropped.
- *Splitting procedure:* The posts considered span a time interval from February 17th, 2023 (t_{start}) to March 18th, 2024 (t_{end}). Key time points are taken as:
 - t_A : December 11th, 2023;
 - t_B : January 22nd, 2024;
 - t_C : February 20th, 2024.

B. Experimental setup

Similar to Bechler-Speicher et al. [2025], we provide an encoder-processor-decoder architecture for all tasks, which we detail in the following. While task-specific parts of our architecture vary, we offer a general architecture to measure the performance of selected baselines on our tasks. For the chip design and weather forecast dataset, we adapt this architecture to provide the necessary task-dependent encoder and decoder functionality.

Encoder For each task, we provide a task-specific encoder that derives encodings for node- and edge-level features with a common dimension $d \in \mathbb{R}^+$. These features are then passed to the processor using node and or edge features. For models that require tokenized input, we provide node-level tokens. For missing node or edge features, a learnable vector of dimension d is used in their place. In case of the GT baseline, we add a [cls] token for graph-level representations, following Bechler-Speicher et al. [2025].

Processor As our processor, we select one of the baseline models we evaluate. These consist of two dummy baselines: an MLP and a DeepSet architecture, a GNN baseline given by a GIN architecture, and a GT baseline. Independent of the selected baseline, we compute updated node and graph representations at each layer as follows, given a graph G with node representations \mathbf{X} ,

$$\mathbf{X} = \phi(\text{LayerNorm}(\mathbf{X}), G) \quad (3)$$

$$\mathbf{X} = \mathbf{X} + \text{MLP}(\text{LayerNorm}(\mathbf{X}))$$

with the following FNN layer:

$$\text{FNN}(\mathbf{x}) := \sigma(\text{LayerNorm}(\mathbf{x}) \mathbf{W}_1) \mathbf{W}_2,$$

where σ denotes the GeLU nonlinearity and $\mathbf{W}_1, \mathbf{W}_2$ are weight matrices. Further, ϕ is the selected baseline, and NNN denotes a two-layer feed-forward neural network with GELU nonlinearity [Hendrycks and Gimpel, 2016]. For the GT baseline, we employed biased attention as described by Bechler-Speicher et al. [2025]. Furthermore, we incorporate RWSE [Dwivedi et al., 2022b] and LPE [Müller and Morris, 2024] as node positional encodings for our MPNN and GT baselines.

Decoder Since every task requires task-specific predictions, we provide a decoder for each. In all functions, we use the same decoder layout, differing only in the predictions. We propose a decoder two-layer multilayer perceptron for our baseline models consisting of two linear layers $\mathbf{W}_1 \in \mathbb{R}^{d \times d}$, $\mathbf{W}_2 \in \mathbb{R}^{d \times o}$ as well as GELU non-linearity, with o denoting the task-specific output dimension, i.e.,

$$\mathbf{W}_2(\text{LayerNorm}(\text{GELU}(\mathbf{W}_1 \mathbf{x}))).$$

Optionally, a bias term can be added to the decoder.

Pretraining In addition to training models with our encoder-processor-decoder architecture, we provide support for task evaluation of pretrained models. These are further specified in the subsections on additional evaluation benchmarks.

Evaluation protocol Using the aforementioned hyperparameter tuning process, we evaluate all baseline models across three random seeds per task and report their mean performance and standard deviations. For out-of-distribution generalization tasks, we utilize pretrained models from these baseline evaluations.

Moreover, we report metrics such as memory usage, training wall-clock time, and inference latency to provide insights into the real-world applications of our benchmark tasks.

B.1. Hyperparameter selection

Here, we provide the hyperparameters used in training our baseline models for each task. We note that in most cases, no extensive hyperparameter search was conducted for the baseline models.

Table 22: List of hyperparameters used for baseline models in BlueSky datasets.

Hyperparam.	Variable	GNN _{quotes}	MLP _{quotes}	Deep Sets _{quotes}	GNN _{replies}	MLP _{replies}	Deep Sets _{replies}	GNN _{reposts}	MLP _{reposts}	Deep Sets _{reposts}
General	Learning rate	1e-3	1e-3	1e-3	1e-3	1e-3	1e-3	1e-3	1e-3	1e-3
	Weight decay	0.	0.	0.	0.	0.	0.	0.	0.	0.
	Dropout	0.	0.2	0.	0.	0.	0.	0.	0.2	0.2
	Epochs	1 000	1 000	1 000	1 000	1 000	1 000	1 000	1 000	1 000
Architecture	Layers	4	2	4	4	4	4	4	2	2
	Hidden dim.	128	128	128	128	128	128	128	128	128

Table 23: List of hyperparameters used for baseline models in SAT solving tasks. These include parameters for positional encoding (PE), the architecture (GIN), and general learning parameters.

Hyperparam.	Variable	GIN _{EPM: VG}	GT _{EPM: VCG}	GIN _{EPM: LCG}	GIN _{AS: VG}	GT _{AS: VCG}	GIN _{AS: LCG}
General	Learning rate	1e-3	1e-3	1e-5	1e-5	1e-5	1e-5
	Batch size	16	16	16	16	16	16
	Weight decay	0.1	0.1	0.1	0.1	0.1	0.1
	Dropout	0.0	0.0	0.0	0.0	0.05	0.0
	Steps	100 000	100 000	100 000	100 000	100 000	100 000
Optimizing	Warmup steps	10 000	10 000	10 000	10 000	10 000	10 000
	Scheduler	CosineAnnealingLR					
	Optimizer	AdamW, betas=(0.9,0.999)					
	Param.	2.2M	2.2M	2.2M	2.2M	2.2M	2.2M
PE	Type	None	None	None	None	None	None
	Encoding dim.	384	384	384	384	384	384
	Hidden dim.	384	384	384	384	384	384
Architecture	Layers	6	16	6	16	6	16
	Hidden dim.	384	384	384	384	384	384
	Activation	GELU	GELU	GELU	GELU	GELU	GELU

B.2. Baseline architectures

In the following, we provide implementation details on the baselines used for the datasets in `GRAPHBENCH`. For dataset-specific design choices, we provide detailed information in Section B.3.

Table 24: List of hyperparameters used for baseline models in algorithmic reasoning tasks. These include parameters for positional encoding (PE), architecture (GT/GIN), and general learning parameters. The respective abbreviations denote the following tasks: topological sorting (TO), minimum spanning tree (MST), bridges (BR), and Steiner tree (ST).

Hyperparam.	Variable	GIN _{TO}	GT _{TO}	GIN _{MST}	GT _{MST}	GIN _{BR}	GT _{BR}	GIN _{ST}	GT _{ST}
General	Learning rate	1e-4	1e-4	3e-4	3e-4	2e-4	2e-4	1e-4	1e-4
	Batch size	256	256	256	256	256	256	256	256
	Weight decay	0.1	0.1	0.1	0.1	0.1	0.1	0.1	0.1
	Dropout	0.1	0.1	0.1	0.1	0.1	0.1	0.1	0.1
	Steps	11 880	11 880	11 880	11 880	11 880	11 880	11 880	11 880
Optimizing	Warmup steps	1 000	1 000	1 000	1 000	1 000	1 000	1 000	1 000
	Scheduler	CosineAnnealingLR							
	Optimizer	AdamW, betas=(0.9,0.999)							
	Param.	2.55M	14.93M	2.68M	15.07M	2.55M	14.93M	2.55M	14.93M
PE	Type	RWSE	RWSE	LPE	LPE	RWSE	RWSE	RWSE	RWSE
	Num. steps/Eigvals	16	16	32	32	16	16	16	16
	Encoding dim.	384	384	384	384	384	384	384	384
	Hidden dim.	768	768	384	384	768	768	768	768
	Num. enc. layers	2	2	2/2	2/2	2	2	2	2
Architecture	Layers	6	16	6	16	6	16	6	16
	Hidden dim.	384	384	384	384	384	384	384	384
	Attn. heads	0	16	0	16	0	16	0	16
	Activation	GELU	GELU	GELU	GELU	GELU	GELU	GELU	GELU

Graph transformer architecture As described in Section B we use an encoder-processor-decoder baseline across tasks. In this case, we consider a GT as the processor architecture following the implementation outlined in Bechler-Speicher et al. [2025]. For most tasks, we use node-level tokenization, treating each graph node as a single token input to the GT. However, for edge-level tasks, we use the transformation outlined for algorithmic reasoning tasks, allowing edge-level tokens to be used without changes to the processor architecture. Additionally, absolute PEs, such as RWSE or LPE, are added to the node embeddings before the first GT layer. Then, the GT layer computes full multi-head scaled-dot-product attention, adding an attention bias B to the unnormalized attention matrix and applying softmax. Let $\mathbf{Q}, \mathbf{K}, \mathbf{V} \in \mathbb{R}^{L \times d}$ and $B \in \mathbb{R}^{L \times L}$ with L denoting the number of tokens and d the embedding dimension. Then, attention and a GT layer take the form

$$\text{Attention}(\mathbf{Q}, \mathbf{K}, \mathbf{V}, B) := \text{softmax}(d^{-\frac{1}{2}} \cdot \mathbf{Q} \mathbf{K}^T + B) \mathbf{V},$$

$$\mathbf{X}^{(t+1)} := \text{MLP}(\text{Attention}(\mathbf{X}^{(t)} \mathbf{W}_Q, \mathbf{X}^{(t)} \mathbf{W}_K, \mathbf{X}^{(t)} \mathbf{W}_V, B)),$$

where $\mathbf{W}_Q, \mathbf{W}_K, \mathbf{W}_V \in \mathbb{R}^{d \times d}$ are learnable weight matrices and MLP denotes a two layer-MLP. In practice, we compute attention over multiple heads, allowing for different attention biases to be added to the attention matrix. With ϕ given by the multihead attention computation, a processor layer is provided by Equation (3). In the processor, multiple layers are stacked, allowing the pipeline shown in Section B.

GIN architecture Throughout this work, we use a GINE-based graph neural network baseline as the processor in the framework outlined in Section B. Following, Hu et al. [2020b] the GINE layer

Table 25: List of hyperparameters used for baseline models in algorithmic reasoning and weather forecasting tasks. These include parameters for positional encoding (PE), architecture (GT/GIN), and general learning parameters. The following tasks are denoted by the respective abbreviations: max clique (MC), flow (FL), maximum matching (MM), and weather forecasting (WE).

Hyperparam.	Variable	GIN _{MC}	GT _{MC}	GIN _{FL}	GT _{FL}	GIN _{MM}	GT _{MM}	GT _{WE}
General	Learning rate	1e-4	1e-4	1e-4	1e-4	1e-4	1e-4	1e-4
	Batch size	256	256	256	256	256	256	16
	Weight decay	0.1	0.1	0.1	0.1	0.1	0.1	0.1
	Dropout	0.1	0.1	0.1	0.1	0.1	0.1	0.1
	Steps	11 880	11 880	11 880	11 880	11 880	11 880	8 000
Optimizing	Warmup steps	1 000	1 000	1 000	1 000	1 000	1 000	500
	Scheduler				CosineAnnealingLR			
	Optimizer				AdamW	betas=(0.9,0.999)		
	Param.	2.68M	15.07M	2.55M	14.93M	2.55M	14.93M	15.35M
PE	Type	LPE	LPE	RWSE	RWSE	RWSE	RWSE	None
	Num. steps/Eigvals	16	16	32	32	16	16	0
	Encoding dim.	384	384	384	384	384	384	384
	Hidden dim.	384	384	768	768	768	768	768
	Num. enc. layers	2/2	2/2	2	2	2	2	2
Architecture	Layers	6	16	6	16	6	16	16
	Hidden dim.	384	384	384	384	384	384	384
	Attn. heads	0	16	0	16	0	16	16
	Activation	GELU	GELU	GELU	GELU	GELU	GELU	GELU

Table 26: List of hyperparameters used for baseline models in CO tasks. These include parameters for positional encoding (PE), architecture (GT/GIN), and general learning parameters.

Hyperparam.	Variable	GIN	GT	MLP	DeepSet
General	Learning rate	1e-3	1e-3	1e-3	1e-3
	Batch size	256	256	256	256
	Weight decay	0.	0.	0.	0.
	Dropout	0.	0.	0.	0.
	Epochs	1 000	1 000	1 000	1 000
	Patience	100	100	100	100
Optimizing	Warmup steps	0	0	0	0
	Optimizer	Adam	Adam	Adam	Adam
	Param.	2.1M	5.6M	1.2M	2.1M
PE	Type	RWSE	RWSE	RWSE	RWSE
	Num. steps/Eigvals	16	16	16	16
	Encoding dim.	384	384	384	384
	Hidden dim.	384	384	384	384
	Num. enc. layers	2	2	2	2
Architecture	Layers	6	6	6	6
	Hidden dim.	384	384	384	384
	Attn. heads	0	4	0	0
	Activation	GELU	GELU	GELU	GELU

Table 27: List of hyperparameters used for baseline models in Electronic circuits tasks. These include parameters for the choice of architecture (GT/GIN/GCN/GAT) and general learning parameters.

Hyperparam.	Variable	GT	GIN	GCN	GAT
General	Learning rate	1e-3	1e-3	1e-3	1e-3
	Batch size	512	512	512	512
	Weight decay	0.	0.	0.	0.
	Dropout	0.	0.	0.	0.
	Epochs	7 00	7 00	7 00	7 00
Architecture	Layers	6	4	4	4
	Hidden dim.	384	384	384	384
	Attn. heads	0	4	0	0
	Activation	GELU	RELU	RELU	RELU

updates the node representations $h_v^{(t)}$ at iteration t as follows:

$$h_v^{(t+1)} = \text{FNN}\left((1 + \epsilon)h_v^{(t)} + \sum_{u \in N(v)} \text{ReLU}(h_v^{(t)} + e_{uv})\right)$$

where $N(v)$ denotes the neighborhood of a node v and FNN is a neural network such as a feed-forward neural network.

We apply the GINE processor layer in a similar way to the GT baseline design outlined previously, by replacing ϕ with a GINE layer with N determined by a dropout layer. First, the node embeddings, optionally with added PEs, are passed to the GINE layer, where layer normalization is applied. The output of the GINE message-passing layer is then forwarded to a two-layer MLP. We use the same residual connection as seen in the GIN implementation from Bechler-Speicher et al. [2025]. We then stack multiple layers together to provide the processor part of our baseline architecture. Unless otherwise specified, we use mean pooling for graph-level tasks at the end of the processor step.

B.3. Architecture choices for datasets

Social networks On the proposed BlueSky datasets, we opted for a different MPNN architecture. The high(er) number of nodes, along with high average node degree and variance, pushed us towards resorting to a message-passing architecture aggregating messages over neighborhoods via averaging (instead of summation as in GIN). We opted, in particular, for a variant of GraphConv with mean aggregation. Node representations $h_v^{(t)}$ are, namely, updated as follows:

$$h_v^{(t+1)} = \sigma\left(W_1^{(t)}h_v^{(t)} + \frac{1}{\deg_{\text{in}}(v)} \sum_{u: u \rightarrow v} W_2^{(t)}h_u^{(t+1)}\right), \quad (4)$$

where σ is set to ReLU, dropout is applied before its application, and, finally, no normalization layers are interleaved.